# The ETNA mission concept: Assessing the habitability of an active ocean world

Ariel N Deutsch, Paolo Panicucci, Laura I Tenelanda-Osorio, Victoria da Poian, Yun H Cho, Chandrakanth Venigalla, Thasshwin Mathanlal, Emiliano Castillo Specia, Graciela González Peytaví, Andrea Guarriello, et al.

frontiers | Frontiers in Astronomy and Space Sciences

TYPE Original Research
PUBLISHED 14 December 2022
DOI 10.3389/fspas.2022.1028357



OPEN ACCESS

EDITED BY
Paolo Cappuccio,
Sapienza University of Rome, Italy

REVIEWED BY
Francis Nimmo,
University of California, Santa Cruz, United States
Anton Ermakov,
University of California, Berkeley, United States

*CORRESPONDENCE
Ariel N. Deutsch,
ariel.deutsch@nasa.gov

†PRESENT ADDRESS
Ariel N. Deutsch,
NASA Ames Research Center, Moffett Field, CA, United States

†These authors have contributed equally to this work and share first authorship

SPECIALTY SECTION
This article was submitted to Planetary Science, a section of the journal Frontiers in Astronomy and Space Sciences

RECEIVED 25 August 2022
ACCEPTED 21 November 2022
PUBLISHED 14 December 2022

CITATION
Deutsch AN, Panicucci P, Tenelanda-Osorio LI, Da Poian V, Cho YH, Venigalla C, Mathanlal T, Castillo Specia E, González Peytaví G, Guarriello A, Gunasekara O, Jones L, Krasteva M, Pouplin J, Villanueva N and Zaref S (2022), The ETNA mission concept: Assessing the habitability of an active ocean world. *Front. Astron. Space Sci.* 9:1028357. doi: 10.3389/fspas.2022.1028357



# The ETNA mission concept: Assessing the habitability of an active ocean world

Ariel N. Deutsch[1,2*†‡], Paolo Panicucci[3†], Laura I. Tenelanda-Osorio[4], Victoria Da Poian[5], Yun H. Cho[6], Chandrakanth Venigalla[7], Thasshwin Mathanlal[8], Emiliano Castillo Specia[9], Graciela González Peytaví[10], Andrea Guarriello[11], Onalli Gunasekara[12], Lewis Jones[13], Mariya Krasteva[14], Jennifer Pouplin[15], Nicole Villanueva[16] and Sam Zaref[17]

[1]Brown University, Providence, RI, United States, [2]NASA Ames Research Center, Moffett Field, CA, United States, [3]Politecnico di Milano, Milano, Italy, [4]Universidad Eafit, Medellín, Colombia, [5]NASA Goddard Space Flight Center, Greenbelt, MD, United States, [6]University of Sheffield, Sheffield, United Kingdom, [7]University of Colorado Boulder, Boulder, CO, United States, [8]University of Aberdeen, Aberdeen, Scotland, United Kingdom, [9]Instituto Tecnológico y de Estudios Superiores de Monterrey, Querétaro, Mexico, [10]Universität der Bundeswehr München, Institute of Space Technology and Space Applications, Neubiberg, Germany, [11]Institut d'Electronique et des Technologies du numéRique–INSA of Rennes, France, [12]University of Illinois Urbana Champaign, Illinois, United States, [13]California Institute of Technology, Pasadena, California, United States, [14]European Space Agency, Noordwijk, Netherlands, [15]Purdue University, West Lafayette, Indiana, United States, [16]Peruvian Space Agency, Lima, Peru, [17]Rhode Island School of Design, Providence, RI, United States

Enceladus is an icy world with potentially habitable conditions, as suggested by the coincident presence of a subsurface ocean, an active energy source due to water-rock interactions, and the basic chemical ingredients necessary for terrestrial life. Among all ocean worlds in our Solar System, Enceladus is the only active body that provides direct access to its ocean through the ongoing expulsion of subsurface material from erupting plumes. Here we present the Enceladus Touchdown aNalyzing Astrobiology (ETNA) mission, a concept designed during the 2019 Caltech Space Challenge. ETNA's goals are to determine whether Enceladus provides habitable conditions and what (pre-) biotic signatures characterize Enceladus. ETNA would sample and analyze expelled plume materials at the South Polar Terrain (SPT) during plume fly-throughs and landed operations. An orbiter includes an ultraviolet imaging spectrometer, an optical camera, and radio science and a landed laboratory includes an ion microscope and mass spectrometer suite, temperature sensors, and an optical camera, plus three seismic geophones deployed during landing. The nominal mission timeline is 2 years in the Saturnian system and ~1 year in Enceladus orbit with landed operations. The detailed exploration of Enceladus' plumes and SPT would achieve broad and transformational Solar System science related to the building of habitable worlds and the presence of life elsewhere. The nature of such a mission is particularly timely and relevant given the recently released *Origins, Worlds, and Life: A Decadal Strategy for Planetary Science and Astrobiology 2023–2032*, which includes a priority recommendation for the dedicated exploration of Enceladus and its habitable potential.

KEYWORDS

Enceladus, habitability, astrobiology, biosignatures, mission concept, seismic network, plume sample analysis, New Frontiers

# 1 Introduction

Are we alone? The presence of contemporary habitats elsewhere in the Solar System with the ingredients necessary to sustain life is a driving force for scientific exploration. Where do these habitats exist, and do organisms live there now? One of the most promising targets to explore these questions is Enceladus, an icy moon of Saturn where a liquid water ocean exists between a dynamic icy shell and a potentially active silicate interior (Brown et al., 2006; Hansen et al., 2006; Porco et al., 2006; Parkinson et al., 2008; Spencer and Nimmo, 2013; Iess et al., 2014; Thomas et al., 2016).

Enceladus Touchdown aNalyzing Astrobiology (ETNA; Figure 1) is a mission concept designed and proposed during the fifth Caltech Space Challenge (CSC) (https://www.spacechallenge.caltech.edu/past-challenges), which is a week-long space mission design challenge that brings together students from across the world to create a pre-Phase A concept study (Rabinovitch et al., 2014). Under the mentorship of experts from NASA, academia, and industry, our team (consisting of 16 students from eight different countries) designed a mission to address the CSC prompt to "assess whether Enceladus provides the conditions necessary (or sufficient) to sustain biotic or pre-biotic chemistry." The CSC dictated five key mission constraints:

1) Land as close as possible to the plumes' sources.
2) Use a collection of small landers/rovers.
3) Target a New Frontiers-class mission arriving at Enceladus between 2036 and 2042.
4) Comply with planetary protection guidelines.
5) Launch the mission with one SLS-type launcher.

We named our mission concept after Mount Etna, which, according to ancient mythology, is where the Greek Giant Enceladus was buried during an epic battle for control of the Cosmos. Mount Etna, like Enceladus, is known for its volcanic and seismic activity.

In this contribution, we discuss the astrobiological potential of Enceladus (Section 2), the importance and relevance of Enceladus exploration in the context of broader Solar System science (Section 3), and the ETNA Science Goals (Section 4), sampling strategy (Section 5), payload (Section 6), mission analysis and concept of operations (conops; Section 7), and spacecraft design (Section 8).

# 2 Astrobiological potential of Enceladus

Enceladus became a compelling exploration target when the Voyager spacecraft (Smith et al., 1982) revealed it to be our Solar System's most reflective body, suggesting the surface is composed entirely of fresh snow or ice (Cruikshank, 1980; Verbiscer et al., 2005; Henin, 2018). Images acquired by Voyager exposed a unique surface reshaped by extensional, compressional, and strike-slip faulting, suggestive of an active interior (Kargel and Pozio, 1996). The Cassini spacecraft (Gautier and Ip, 1984) since confirmed Enceladus is an active world, imaging active plumes erupting material sourced from beneath the south polar terrain (SPT) and expelling it tens of kilometers into space (Hansen et al., 2006; Spahn et al., 2006; Hsu et al., 2015; Waite et al., 2017; Postberg et al., 2018). Targeted flybys by Cassini revealed enhanced thermal anomalies associated with the erupting plumes, suggesting the plume activity is driven by tidal stresses and convective heating of the ice shell (Roberts and Nimmo, 2008; Běhounková et al., 2017). The correlation between individual plumes and small (~10 m) hot spots suggests latent heat is transported from a subsurface ocean (Goguen et al., 2013; Porco et al., 2014). Various geophysical measurements also support the presence of a stable, long-lived subsurface ocean beneath the ice shell (McKinnon, 2015; Thomas et al., 2016; Čadek et al., 2016), which is estimated to be 30–40-km thick on average (Iess et al., 2014; McKinnon, 2015; Hemingway and Mittal, 2019) but only a few-km thick in the SPT (Beuthe et al., 2016; Čadek et al., 2016; Le Gall et al., 2017), where the moon's active plumes and tiger stripes are located. The tiger stripes are a pattern of long fractures extending hundreds of kilometers that appear to be linked to the tidal and eruption cycles of Enceladus (Hurford et al., 2007; Nimmo et al., 2014).

Of particular astrobiological interest, Cassini captured expelled plume material during flybys and analyzed its composition (Waite et al., 2006, 2017; Tokar et al., 2009; Teolis et al., 2010; Postberg et al., 2018), revealing the plumes to be composed predominantly of water vapor, along with hydrogen gas and some heavier trace compounds of organic molecules, including nitrogen, carbon dioxide, methane, propane, and acetylene, which may be conducive to the origin and evolution of life (Porco et al., 2006; Waite et al., 2009). In fact, some of the plume components have been identified in hydrothermal systems on Earth, and comparisons with Enceladus can serve to test the hypothesis of the origin of life in these systems (Martin and Russell, 2007; Russell et al., 2014). The plume materials are presumably sourced from Enceladus' subsurface ocean (Porco et al., 2006; Spencer and Nimmo, 2013; Waite et al., 2017; Postberg et al., 2018),

which has sea floor pressures similar to those at terrestrial oceanic depths of ~1000 m (NRC, 2022). Frozen droplets of water in the plume have a salinity and alkaline pH comparable to terrestrial oceans (Postberg et al., 2011; Glein et al., 2015; Glein and Waite, 2020), where early life may have evolved on our own planet (Sverjensky and Lee, 2010; Pope et al., 2012). Plume materials also contain tiny silica grains, which likely originate from ongoing high-temperature water-rock reactions made possible from tidal heating below the ocean floor (Postberg et al., 2011; Hsu et al., 2015; Postberg et al., 2018), an environment suitable for aqueous catalytic chemistry (Matson et al., 2007). Ongoing water-rock interactions at depth are further implied by the ocean's alkaline pH, sodium and potassium salts, and a low-density rocky core (Glein et al., 2015; Hsu et al., 2015; Zandanel et al., 2021; Kang et al., 2022).

Today, outstanding questions remain regarding the habitability (and occupancy) of Enceladus. For example, although organics have been measured in Enceladus' erupted plume material, the limited resolution and high altitude of Cassini's mass spectrometer prevented detailed measurements of heavier organics, and some organic matter is expected to have broken down during the high-speed fly-by collections (Waite et al., 2009; Postberg et al., 2018). Heavier compounds are of critical importance to assess (pre-) biotic signatures (McKay et al., 2014). Furthermore, P and S were not detectable by the mass spectrometer (Postberg et al., 2011), but are needed to complete the biomarker inventory of CHNOPS (Hill, 2000).

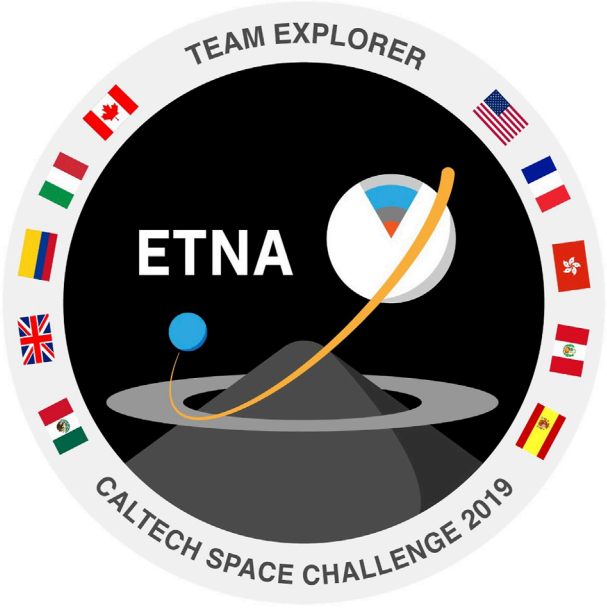


FIGURE 1
The Enceladus Touchdown aNalyzing Astrobiology (ETNA) mission was designed by our team of 16 students representing eight different countries. Mission patch and artwork designed by Sam Zaref.

## 3 Relevance to NASA

Enceladus is a compelling target to study astrobiology and habitability in our Solar System because it is an active body that provides direct access to its ocean through the expulsion of subsurface material (NRC, 2011, 2022; Cable et al., 2021a; Choukroun et al., 2021; Mathies and Butterworth, 2021; Vance et al., 2021). ETNA was designed to address two main scientific questions outlined by the CSC prompt: "Does Enceladus provide habitable conditions?" and "What (pre-) biotic or abiotic signatures characterize Enceladus?" These Science Goals directly address the question "How did life begin and evolve on Earth, and has it evolved elsewhere in the Solar System?" which was identified by NASA's Science Mission Directorate to motivate Solar System exploration (https://science.nasa.gov/solar-system/big-questions/).

The ETNA mission was conceived in 2019, under the context of the *Vision and Voyages for Planetary Science in the Decade 2013–2022* (NRC, 2011). At that time, our team determined ETNA directly responds to two of the three identified cross-cutting science themes of the 2013–2022 Decadal: "Planetary Habitats" and "Workings of Solar Systems". The 2013–2022 Decadal specifically recommended Enceladus as one of four exploration targets that hold the greatest potential as modern habitats for Earth-like life. ETNA takes advantage of the unique opportunity to directly sample subsurface compounds from an active hydrologic system with plume fly-throughs and subsequent landed sample collection, allowing for the analysis of materials expelled from Enceladus' subsurface ocean.

Since the conception of ETNA, the National Academies released the *Origins, Worlds, and Life: A Decadal Strategy for Planetary Science and Astrobiology 2023–2032* (NRC, 2022). With this new Decadal, the recommendation for a dedicated Enceladus mission has elevated, and Enceladus science aligns with various Priority Science Questions within the Decadal Scientific Themes of "Life and Habitability" and "Worlds and Processes" (NRC, 2022). The Decadal committee specifically recommended an Enceladus "Orbilander" mission (MacKenzie et al., 2020, 2021) as the second-highest priority for a new Flagship mission. Orbilander has many common elements with ETNA; it would analyze fresh plume material from orbit and during a landed phase to 1) search for evidence of life and 2) obtain geochemical and geophysical context for life detection experiments. If Orbilander is not supported, the Decadal recommends NASA invests in an Enceladus multiple flyby mission to progress icy ocean world and habitability science. Thus, continuing to explore Enceladus in detail is a driving priority in the upcoming decade, and would be enabled with a

TABLE 1 ETNA Science Goals and Objectives, and their relevance to Decadal Survey Priority Questions.

| ETNA Science Goal | ETNA Science Objective | 2013–2022 Decadal Priority Questions addressed | 2023–2032 Decadal Priority Questions addressed |
|---|---|---|---|
| 1. Does Enceladus provide habitable conditions? | 1A Determine the bulk chemical composition of the subsurface | 4, 6,10 | 5 |
| | 1B Determine what energy sources drive surface and subsurface interactions | 4, 6, 10 | 5 |
| | 1C Determine the periodicity and lifetime of habitable conditions | 4, 6, 10 | 10 |
| 2. What (pre-)biotic or abiotic signatures characterize Enceladus? | 2A Characterize the composition, structure, and ratios of plume materials | 4, 6, 10 | 10, 11 |
| | 2B Determine if visual biomarkers are present in erupted plume materials | 4, 6 | 10, 11 |
| | 2C Determine how CHNOPS are produced | 4, 6 | 10, 11 |

mission such as ETNA, Orbilander (MacKenzie et al., 2020), "SILENUS" (Spectrometer Investigating the Livability of Enceladus with a Network of Underground Seismometers) as designed by another CSC team (Nathan et al., 2022; this issue), or "EnEx" (Enceladus Explorer; Konstantinidis et al., 2015). Table 1 specifies how ETNA Science Goals and Objectives directly map to the Priority Questions outlined in the two most recent Decadal Surveys (NRC, 2011; NRC, 2022).

# 4 Driving science

Here we outline Science Goals of the ETNA mission, which are presented in a Science Traceability Matrix in Figure 2, and were designed to address the CSC mission prompt (Section 1).

## 4.1 Science Goal 1: Does Enceladus provide habitable conditions?

The first Science Goal is related to characterizing the habitability of Enceladus and determining how habitable conditions are provided and sustained (Hoehler et al., 2021). This goal provides key geochemical and geophysical context in the search for (pre-) biotic signatures. Addressing this goal would allow us to quantify the biomass that Enceladus could support by constraining the ocean's temperature, salinity, pH, nutrient availability, and energy sources (Glein and Waite, 2020; Cable et al., 2021a; MacKenzie et al., 2021). It would also allow us to constrain the timescales of habitable conditions, providing insight into the favorability of developing high Pathway Complexity Indices (Marshall et al., 2017). Science Goal 1 is defined by three Science Objectives (Figure 2).

### 4.1.1 Objective 1A: Determine the bulk chemical composition of the subsurface

It is known that the plume materials contain chemical ingredients that characterize habitable environments, including native hydrogen, water vapor, and simple organic compounds (Waite et al., 2006, 2017; Kahana et al., 2019; Hansen et al., 2020), but questions remain regarding the presence of phosphorus and sulfur (two key biomarkers of terrestrial life; Postberg et al., 2011) and heavy organic compounds, which are suggestive of more complex chemical reactions and possibly biologic activity (Waite et al., 2009; McKay et al., 2014; Barge and Rodriguez, 2021). To address these unknowns and investigate the composition of Enceladus' ocean, ETNA would collect and analyze ejected plume materials. Analyzing the bulk chemical composition of plume materials would provide insight into potential sources and pathways for Enceladus' chemistry. ETNA would determine the:

1) Presence and relative abundance of CHNOPS, organic, and inorganic species in plume materials.
2) Spatial variability of the composition of erupted plume materials.
3) Abundance of Na and Cl in plume materials for oceanic salinity constraints.

### 4.1.2 Objective 1B: Determine what energy sources drive surface and subsurface interactions

Characterizing the moon's internal structure and bulk parameters is important to assess the energy source(s) of its dynamic plume activity and resurfacing (Hurford et al., 2007; Tian et al., 2007; Hedman et al., 2013; Běhounková et al., 2017; Southworth et al., 2019). ETNA would constrain the:

| Science Goal | Science Objective | Measurement | Instrument | Phase | Functional Requirements |
|---|---|---|---|---|---|
| 1. Does Enceladus provide habitable conditions? | 1A Determine the bulk chemical composition of the subsurface. | Identification and relative abundance of CHNOPS. | IMAMS | O, L | ≥1 μL of plume material collected during flythrough at altitudes <40 km and landed operations. |
| | | Relative abundance and diversity of organic and inorganic species (e.g., salts, silicates, metals, metal hydroxides, sulfates, carbonates) with masses ≤500 Da. | | | |
| | | Abundance of Na and Cl ions for salinity. | | | |
| | 1B Determine what energy sources drive surface and subsurface interactions. | Composition as a function of plume height at <10-mpp resolution. | IMAMS, UVIS | O, L | Repeated coverage of plumes; High-phase-angle images of plumes. |
| | | Ground temperature near an active vent <5-K resolution. | AGTS | L | Land ≤5 km from an active vent. |
| | | Seismic signal location of frequencies from 0.1–240 Hz at ≤1-min sampling. | SHOOC | L | Surface operations for ≥6 days; Geophone location to <5 m accuracy. |
| | | Thickness of crust in SPT with <20-m vertical accuracy and <100-m horizontal wavelength. | SHOOC, RS | O, L | Surface operations for ≥6 days; Geophone location to <5 m accuracy; Repeated polar orbits at altitudes ≤200 km. |
| | | Presence of structural heterogeneities (e.g., vent structures, caverns, reservoirs) with <20-m vertical resolution. | | | |
| | | Tidal love numbers, with $k_2$ accuracy better than $10^{-3}$. | RS | L | Repeated polar orbits at altitudes ≤200 km. |
| | | Topography of the oceanic floor (gravity field harmonics up to degree 10). | | | |
| | 1C Determine the periodicity and lifetime of habitable conditions. | Topography of SPT with <10-m lateral spatial resolution. | OICAM | O | Polar imaging during illuminated conditions; Repeated coverage. |
| | | (Stereo) imaging of SPT and vent structures with <10-m spatial resolution. | | | |
| | | Rate of plume-material deposition over 10-hour periods. | UVIS, OICAM | O | Plume materials collected during landed operations; High-phase-angle images. |
| | | Mass flux of erupted material. | | | |
| | | Dominant stress direction and magnitudes at frequencies from 0.1–240 Hz. | RS, SHOOC | O, L | Repeated polar obits; Surface operations for ≥6 days; Geophone location to <5 m accuracy. |
| 2. What (pre-)biotic or abiotic signatures characterize Enceladus? | 2A Characterize the composition, structure, and ratios of plume materials. | Relative abundance and diversity of organic and inorganic species (e.g., salts, silicates, metals, metal hydroxides, sulfates, carbonates) with masses ≤500 Da. | IMAMS | O, L | ≥1 μL of plume material collected during flythrough at altitudes <40 km and landed operations. |
| | | Abundances and patterns of organic compounds in the sample plume materials (including amino acids, carboxylic acids, hydrocarbons, and lipids) at concentrations of 1 pmol/μL. | | | |
| | | Chirality and relative abundances of at least three amino acids at 1pmol/microliters, or 1ppbm involved at least in one abiotic, prebiotic, and biotic processes such as: Ala, Asp, His, Leu, Per, Val, Iva, Glycolic, beta-Ala, GABA and AIB. | | | |
| | | Broad weight distribution of organics with masses ≤500 Da. | | | |
| | 2B Determine if visual biomarkers are present in erupted plume materials. | Structure and morphology of plume materials >0.1 μm in diameter. | | | |
| | | Presence of potential biominerals (e.g., silicate, magnetite, iron sulfides, or carbonate) at levels of 1 particle per thousand of mass. | | | |
| | 2C Determine how CHNOPS are produced. | Relative abundance and diversity of organic and inorganic species (e.g., salts, silicates, metals, metal hydroxides, sulfates, carbonates) with masses ≤500 Da. | | | |
| | | CHNOPS isotopologues distribution of the organic and inorganic matter at 1 pmol/μL. | | | |

FIGURE 2
ETNA science traceability matrix.

1) Thickness and heterogeneity of the ocean and ice shell layers, both for the local SPT and for the global structure.
2) Topography of the oceanic floor.
3) Geometries and physical structures of surface vents at the SPT.
4) Mass flux of material erupted from the subsurface to the surface in active plumes.
5) Surface temperature of the SPT and eruption regions.
6) Physical and thermal stresses of the SPT.

Tidal dissipation, which is thought to be linked to Enceladus' ongoing plume activity, is generated by deep-ocean tidal flow across rough seafloor topography, transferring energy to internal waves and eventually smaller-scale dissipative processes (i.e., heat) (Tyler, 2009). Thus, constraining the topography of the seafloor would improve our estimates of regional tidal flow and heat flux. Furthermore, mapping the seafloor topography and the spatial relationships between vents, and possible caverns, chimneys, or other oceanic structures, would enable structural comparisons with oceanic habitats on Earth, where early life evolved (Martin et al., 2008; Shields et al., 2019). Lastly, the relationship between bathymetry and variations in vent abundance and plume activity could provide important insight into pathways between the subsurface and surface.

### 4.1.3 Objective 1C: Determine the periodicity and the lifetime of these habitable conditions

To assess the habitability of Enceladus, it is essential to understand whether favorable conditions persisted long enough to allow for the origin of life (McKay et al., 2008). On Earth, hydrothermal environments can sustain the spontaneous synthesis of simple organic compounds (even in the absence of life) and are known to support some of Earth's most primitive forms of microbial metabolism (NRC, 2022). It is possible that life could have also emerged on Enceladus if its ocean and hydrothermal activity have been sufficiently long-lived.

One approach to constraining the timescales of plume activity is to determine the surface ages of various geologic units on Enceladus. Other geologic terrains have relatively higher crater densities and are interpreted to be older than the SPT (Kirchoff and Schenk, 2009). Some nearby terrains also have a deficiency of craters with diameters ≤2 km,

interpreted to be due to burial by expelled plume materials (Kirchoff and Schenk, 2009). Comparing crater densities of the SPT, of nearby terrains whose crater populations have been altered by plume outfall, and of terrains whose crater populations have not been modified by plume activity can help constrain the relative timescales of how long the plumes have been erupting.

To help constrain the periodicity and lifetime of habitable conditions, ETNA would constrain the:

1) Density and frequency of erupting plumes, and variations through eruption lifetimes.
2) Number and geometries of inactive and active surface fissures.
3) Surface age of the SPT and other geologic units.
4) Mass flux of erupted plume material and rate of resurfacing.
5) Dynamics of vent-driving processes leading to plume eruptions.

## 4.2 Science Goal 2: What (pre-) biotic or abiotic signatures characterize Enceladus?

With Science Goal 2, we seek to find evidence of life from the past, present, or potentially future (i.e., pre-biotic). What is the complexity and progression of organic chemistry on Enceladus? This goal would be addressed through the search for various biosignatures to help constrain if and to what extent life has evolved on the moon. Science Goal 2 is defined by three Science Objectives (Figure 2).

### 4.2.1 Objective 2A: Characterize the composition, structure, and ratios of plume materials

In addition to characterizing the processes that have shaped Enceladus as a habitable world, ETNA was designed to determine if there are any (pre-) biotic signatures. Understanding the geochemistry of these plumes can provide critical insight into the geochemistry of the ocean (Matson et al., 2007; Zolotov, 2007; Glein et al., 2018) and the potential habitability of Enceladus (McKay et al., 2008, 2014; Parkinson et al., 2008; Barge and Rodriguez, 2021). ETNA would investigate the presence of biologic signatures by assessing the composition, patterns, and chemical and structural complexity of expelled plume materials (both particulate and vapor) (Knoll, 2003; Higgs and Pudritz, 2009; Domagal-Goldman et al., 2016).

The abundance and structural patterns of amino acids and lipids as a function of carbon chain length can be used to distinguish between abiotic and biotic sources (Summons et al., 2008; Georgiou and Deamer, 2014). The "Pathway Complexity Index" would be computed to index the level of organic molecule complexity in plume samples, and to discriminate between abiotic and biotic processes (Marshall et al., 2017). Because this index does not make any assumptions about the nature of the biochemistry at work, it is agnostic toward the type of life that may have evolved on a planetary body (Marshall et al., 2017).

Chirality also provides insight into biological vs nonbiological origins (Glavin et al., 2020). In terrestrial systems, biotic amino acids tend to exhibit left-handed homochirality while abiotic amino acids lack a strong preference. Combining measurements of amino acid relative abundance, chirality, and isotopic abundances provides the strongest case of measuring biologic origin (Glavin et al., 2020). Therefore, in analyzing collected plume materials, ETNA would:

1) Determine the composition (including Cl-containing compounds, sulfates, carbonates, silica, silicates, and metal oxides).
2) Determine the abundances, broad weight distribution, and patterns of organic compounds (including amino acids, carboxylic acids, hydrocarbons, and lipids).
3) Compare the composition, abundance, and distribution of organic compounds to databases of terrestrial organic compounds.
4) Measure the chirality and abundance of amino acids.

### 4.2.2 Objective 2B: Determine if visual biomarkers are present in erupted plume materials

The most robust detection of biotic signatures would derive from independent, repeatable measurements of biosignatures (Neveu, 2016; Hand et al., 2017; Neveu et al., 2018). Thus, in combination with chemical measurements of plume materials (Objective 2A), ETNA would also search for visual biomarkers (Simoneit, 2002, 2004). All living cells possess a membrane made of lipids that aid in the exchange of material, communication, energy conservation, and protection from thermal and mechanical stresses, and these structures can be visually identified (Stoeckenius, 1962; Bretscher, 1985; Watteau and Villemin, 2018) and experimental work suggests that the morphological integrity of cells could be preserved during plume ejection (Bywaters et al., 2020). While the detection of cell-like structures would not offer conclusive evidence of life (Schopf, 1993; McKay et al., 1996), such a detection in combination with various chemical biosignatures would present a more robust characterization. ETNA would be capable of assessing biosignatures through visual biomarkers to search for direct observations of cells and biomaterials in plume materials with the following investigations:

1) Characterize micro-scale evidence for life in collected plume materials by searching for cellular and other microstructures (e.g., spores).

2) Identify potential biominerals and fossils (e.g., trapped in grains or layered structures).

#### 4.2.3 Objective 2C: Determine how CHNOPS are produced

Finally, it is critical to determine the source of the elements that form potential (pre-)biotic signatures. What abiotic processes are supporting habitable conditions at Enceladus, both within the ocean and at rock-ice interfaces? Understanding the composition of the erupted plume materials would provide direct information about interior reactions and ocean chemistry (Hansen et al., 2011; Matson et al., 2012; Postberg et al., 2018). Additionally, isotopic ratios would provide important insight into biological origins of chiral asymmetry (Glavin et al., 2020) and the presence of metabolic reactions and any biotically-induced disequilibrium (Shuai et al., 2018; Cao et al., 2019). Therefore, ETNA would determine the:

1) Chemistry of the plume materials.
2) Isotope distributions (including CHNOPS) of the plume materials.

## 5 Plume sampling strategy

Landing on the surface enables a higher scientific return, especially in the context of habitability. To analyze the habitability potential of Enceladus, as well as pre-biotic and biotic measurements, it is critical to investigate both the internal dynamics of the SPT, where the active plumes are observed, and also the composition of ejected oceanic particles. The plumes act as conduits from the subsurface to the surface, transferring oceanic particles from the subsurface liquid water ocean, through the atmosphere, and back to the surface. These particles can be analyzed while lofted or upon atmospheric fallout once they are deposited on the surface. ETNA would capitalize on these opportunities and would collect and analyze materials both during orbital operations *via* a plume fly-through (Section 7.2) and also during surface operations with an *in-situ* landed laboratory (Section 7.3).

### 5.1 Orbital plume sampling

The production rate of water ice by the vent is estimated to be ~30 kg/s on average (Porco et al., 2017; Southworth et al., 2019), although the mass fluxes of jets vary spatially and temporally, even in a single stripe (Teolis et al., 2010). The lighter compounds and vapor particles can sometimes be ejected at such high velocities that they exceed Enceladus' escape velocity (250 m/s) and reach Saturn's E-ring (Schmidt et al., 2008; New et al., 2021). Heavier and larger particles, which are predominantly of astrobiological interest, are ejected at relatively lower velocities and can reach up to 80 km in altitude before resulting in global resurfacing fallout (Hansen et al., 2006; Schmidt et al., 2008; Yeoh et al., 2015; Guzman et al., 2019). Particles with diameters between 1 and 100 μm are estimated to reach altitudes of ~25–50 km. Thus, ETNA's orbital operations include a fly-through of an active plume at an altitude of 25 km. Given Cassini observations (Porco et al., 2006; Waite et al., 2006), we expect multiple plumes would be active during ETNA operations. Our orbital conops does not require that a particular plume is selected before launch; built-in mission flexibility and healthy mass and power budget margins enable our Science Team to select active plumes upon Enceladus arrival. Active plumes would be visible before the spacecraft is inserted into orbit around Enceladus from its onboard camera, so on-ground decisions could be made without haste.

For the IMAMS chemical analysis, the aggregate concentration directly affects the limit of detection (i.e., larger sample volumes improve detection limits; Mathies and Butterworth, 2021). Material is collected during repeated plume fly-throughs until a volume of 1 μl is acquired, sufficient for IMAMS analysis (Figure 2), consistent with the measurement volume requirements of the Orbilander spacecraft (MacKenzie et al., 2020). Previous analyses suggest this volume can be acquired in <two to five orbits, assuming a sample flux of 1.6–6 μl/m/orbit (Porco et al., 2017; Guzman et al., 2019) and taking into consideration our 40-cm-diameter collection plate.

### 5.2 Landed plume sampling

ETNA would also sample expelled plume material during surface operations (Section 7.3). The collection plate remains open while plume fallout is collected. Assuming a fallout rate of 1 mm/year (Southworth et al., 2019), 1 μl could be collected in <20 h.

The landing point should be located 1) close enough to an active vent such that heavy erupted plume materials can be sampled and 2) within a region of elevated thermal emission. We would land the *in-situ* laboratory at a maximum distance of 5 km from an active vent opening. This distance was calculated to be sufficient for the sampling of heavier molecules; beyond this distance, the frequency of such heavier molecules diminishes (Porco et al., 2006; Jaumann et al., 2008).

The specific vent is not a major constraint; the composition of ejected material may be similar between plumes if fed by the same subsurface ocean. Thus, stationary landed operations satisfy ETNA science requirements and there is no need to introduce mission complexity by traveling between multiple vents. The nominal landing point is at the junction point of the Baghdad Tiger Stripe (Figure 3), which is characterized by high plume fallout (Southworth et al., 2019) and low ice-block counts (Martens et al., 2015); but again, built-in mission

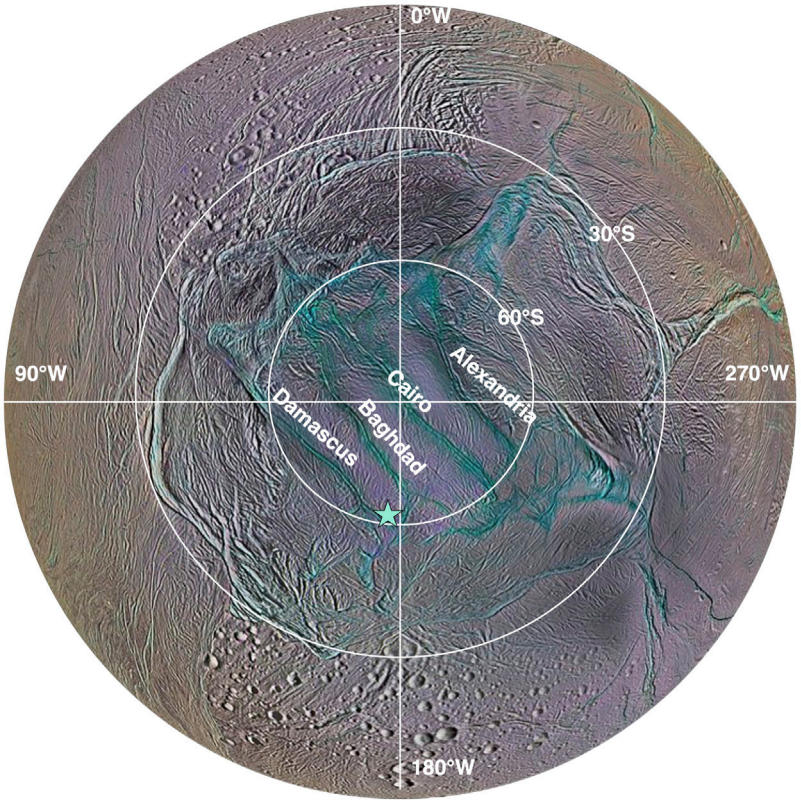


FIGURE 3
Nominal landing site marked by teal star, at the junction of Baghdad. The four southern Tiger Stripes are labeled for reference. Backmap is a mosaic (pixel resolution of 100 m) constructed from Cassini ISS images in polar stereographic projection (Credit: Paul Schenk, LPI).

flexibility and margins support landing site adjustment during operations.

In addition to science considerations, landing site selection should consider engineering safety. For example, the Orbilander concept study (MacKenzie et al., 2020, 2021) addressed the importance of:

1) Landing on a rigid surface to support the mass of the landed laboratory (the presence of large boulders resolved in Cassini images suggests the surface is rigid);
2) Landing on nearly horizontal slopes (<10°) to avoid tipping;
3) Not landing on a surface that has a high density of rocks, ice blocks, and boulders for safety of the laboratory and deployed geophones; and
4) Not landing in a topographic low that would prevent orbiter line-of-sight.

At this time, these additional constraints have not been applied to ETNA's candidate landing site, but we emphasize that the mission architecture is robust to the adjustment and/or re-selection of a SPT landing point. It is likely that the greatest of these four safety constraints would be locating a surface with a paucity of hazards. Ice blocks with sizes ranging from ~10 to 366 m are present in the SPT, with larger blocks tending to be closer to the tiger stripes (Martens et al., 2015; Pajola et al., 2021). However, Martens et al. (2015) identified several areas in the SPT that have low block counts (0–100 blocks/km$^2$), which are favorable for surface operations. Our nominal landing site is one of these areas. Reconnaissance during orbital operations would help ensure low block counts and refine the landing site.

## 6 Enceladus Touchdown aNalyzing Astrobiology payload

To address our Science Goals (Figure 2), ETNA has a scientific payload consisting of six scientific instruments that are split between an orbiter and a landed laboratory, as well as a distributed seismic network consisting of three geophones (Table 2). All instruments have high technology readiness levels (TRLs) except for the geophone seismic network, which

TABLE 2 ETNA science instrument suite. Power and mass estimates are from heritage instruments.

| Instrument | Key parameters and capabilities | Heritage | Max power (W) | Mass (kg) | Spacecraft accommodation | ETNA Science Goal |
|---|---|---|---|---|---|---|
| Ultraviolet Imaging Spectrometer (UVIS) | • Spectral bandpass: 52–187 nm<br>• Observational wavelength: 50–180 nm<br>• Input channels: Airglow and Solar Occultation Channel<br>• SNR: 10 | New Horizons Alice | 4.4 | 4.4 | Mounted on orbiter | 1 |
| Optical and Infrared Camera (OICAM) | Multispectral Visible Imaging Camera (Pushbroom Color Imaging Device)<br>• Wavelengths: 400–975 nm (7 channels)<br>• Modes: panchromatic (400–975 nm), blue (400–550 nm), red (540–700 nm), NIR (780–975 nm), methane (860–910 nm), and navigation/framing array<br>• SNR: 15 for methane channel, 50 for all other (33 AU, 0.35 I/F)<br>Linear Etalon Imaging Spectral Array (IR Imaging Spectrometer)<br>• Wavelengths: 1.25–2.5 μm<br>• Resolution: $\lambda/\Delta\lambda \geq 250$<br>• SNR: 32 (1.25 μm); 27 (2.00 μm); 18 (2.15 μm) | New Horizons Ralph | 7.1 | 10.5 | Mounted on orbiter | 1 |
| Radio Science (RS) | Radio Science<br>• Transmission wavelengths: 14 cm (S-band), 4 cm (X-band), 1 cm (Ka-band) | Cassini Radio Science | 100[a] | 115.5[a] | Mounted on orbiter | 1 |
| Ion Microscope And Mass Spectrometer (IMAMS) | Optical microscope<br>• Spatial sampling: 7 μm<br>IR microscope<br>• Spatial sampling: 5 nm<br>• Spectral range: 1–4 μm<br>Laser desorption/ablation mass spectrometer<br>• Resolution: >120,000 m/Δm<br>• Mass accuracy: ±3.2 ppm<br>• Isotopic abundance precision: <1.0%<br>GCMS/TMS<br>• Resolution: <1 u<br>• Mass accuracy: Observed mass ±0.4 u actual mass<br>• Mass range capability: 50–500 Da | CIVA-M<br>CosmOrbitrap<br>ExoMars MOMA | 90 | 17.6 | Mounted on lander | 1, 2 |
| Lander Inspection Camera | CCD Camera<br>• Monochromatic-diode wavelengths: 470, 530, 640, and 870 nm<br>• Readout rate: 625 kpixel/s<br>• System noise: <1 DN | Rosetta ROLIS | 2.2 | 0.41 | Mounted on lander | 1 |

(Continued on following page)

TABLE 2 (*Continued*) ETNA science instrument suite. Power and mass estimates are from heritage instruments.

| Instrument | Key parameters and capabilities | Heritage | Max power (W) | Mass (kg) | Spacecraft accommodation | ETNA Science Goal |
|---|---|---|---|---|---|---|
| Air and Ground Temperature Sensors (AGTS) | Air Temperature Sensor (2 Minisens RTD thermistors of type PT1000 Class A) + Ground Temperature Sensor (8–14 μm thermopile)<br>• Resolution: 0.1 K (Air), 2 K (Ground)<br>• Accuracy: ± 5 K (Air), 10 K (Ground)<br>• Sampling rate: 1 Hz | Curiosity REMS | 0.1 | 0.04 | Mounted on lander | 1 |
| Seismic geopHOning Oceans and Crusts (SHOOC) | Distributed Seismic Network<br>• Frequency range: 0.1–240 Hz<br>• Operating temperature: 55-125 C | Instrument was designed as part of the CSC, but some components derive from AGEX. | 13 (Nominal: 1) | 48.9 (16.3 per probe)[b] | Carried on and deployed from lander | 1 |

[a]Orbiter communication subsystem power and mass.
[b]The percussor mass is included in the spacecraft design mass.

was designed in response to the CSC requirement of using "a collection" of landed components.

## 6.1 Ion Microscope And Mass Spectrometer Suite

The IMAMS suite would be used to determine the:

1) Chemical composition, chirality, and isotopic ratios of plume material.
2) Relative abundance of amino/fatty/carboxylic acids to glycine of plume material.
3) Mass flux and spatial variability of plume composition.
4) Structure, morphology, and presence of biominerals in plume material.

Sample materials would be passively collected from plumes during the orbiter phase (*via* a plume fly-through) and during the landed phase (*via* plume deposition that falls naturally into the collector located on the top of the lander). The microscope would be the first instrument to receive a collected plume sample. Microscopic images would be used to analyze cell-like morphologies and other potentially biologic microstructures, such as spores. Derived from the Comet (CIVA)-M instrument, the microscope combines two ultra-compact and miniaturized microscopes: a visible microscope and NIR hyperspectral imager (Bibring et al., 2007). The microscope would image the sample from 13 mm away by non-destructive techniques for the analysis of biological structures, as well as texture and albedo (Bibring et al., 2007).

After being imaged by the microscope, the sample would be divided into two sample plates (each requiring only <0.001 μl; MacKenzie et al., 2021; Mathies and Butterworth, 2021) and delivered to two mass spectrometer subsystems: the Gas Chromatography Mass Spectrometer (GCMS) and Tandem Mass Spectrometer (TMS). The GCMS is important for identifying volatile components, assessing chirality, differentiating between isotopes, and determining whether a molecule is from biotic or abiotic origin (Goesmann et al., 2017). The TMS provides complementary mass information for heavier compounds. A precise measurement of mass has the capability of distinguishing between amino acids (Arevalo et al., 2018), which are the building blocks of DNA. The relative concentrations of amino acids derived from biotic sources provide critical information about their functional roles in biotic systems (Dorn et al., 2011; Hand et al., 2017; Glavin et al., 2020; MacKenzie et al., 2020, 2021). Amino acids derived from abiotic sources show comparatively simple patterns comprised of molecules with low-formation-energy requirements (Dorn et al., 2011).

Plume samples would be heated into a gas by the GCMS to separate the different molecules. A derivatization agent applied to the sample tests for chirality. The resulting sample is then sent to a dedicated mass analyzer, which is a tested prototype of a high-end TMS developed specifically for planetary exploration. It uses the same Linear Ion Trap (LIT) as was used on MOMA for ExoMars, as well as a very high-resolution CosmOrbitrap mass analyzer adapted for space applications (Arevalo et al., 2018, 2020). The TMS fragments the sample by ionization using a pulsed UV laser. The optically stabilized ions are directed to the CosmOrbitrap mass analyzer, which determines the mass of the ions by measuring their mass to charge ratio (m/z) by applying a

known magnetic field into the mass analyzer cavity (Arevalo et al., 2018, 2020). Finally, the resulting electrical signal is amplified and sent to the digital processing unit.

## 6.2 UV Imaging Spectrometer

The UV Imaging Spectrometer (UVIS) would be used to:

1) Obtain compositional and morphological information of the surface.
2) Map the composition of the plumes as a function of space and time.
3) Obtain ion abundance measurements of plumes around perihelion.

These data would be used for plume fly-through and landing site selection, and to analyze plume activity with respect to changes in jet morphology and structure. Specifically, images of the plumes at multiple wavelengths would be used to help reconstruct the composition of the plumes. Images would be acquired at multiple times to help reconstruct the dynamic structure, density, and temperature of the plumes as a function of altitude and to make compositional and production rate measurements of plumes.

The UVIS, derived from Alice (Stern et al., 2009), consists of a compact telescope, a spectrograph, and a sensitive electronic detector with 1,024 spectral channels at 32 separate spatial locations in its rectangular field-of-view. It has two modes of operation: an "airglow" mode that measures UV emissions from atmospheric constituents and an "occultation" mode, where it focuses on a star and measures the amount of sunlight absorbed, providing insight into atmospheric constituents between the instrument and star. Thus, stars occulted by the plumes could be observed and used to map the water molecule spatial distribution and provide insight into the location of the production regions.

## 6.3 Optical and Infrared CAMera

The Optical and Infrared CAMera (OICAM) would be used to:

1) Image the surface (including with stereo techniques).
2) Map compositional variations across the surface.
3) Map surface temperature.

The camera would provide important information for characterizing the morphology and morphometry of the SPT, providing key geologic context for the interpretation of other ETNA data sets. OICAM data would be essential in studying the outgassing vent structures, so that vent shape, geomorphology, and texture could be resolved at various plume source regions. Images would also be used to refine surface ages of various geologic terrains to help constrain timescales of plume activity (Section 4.1.3) and to study potential landing sites at high spatial resolution and generate local digital terrain models for landing site preparation.

OICAM is a VIS/NIR multispectral imager (with panchromatic and color imaging capabilities) and a short-wavelength IR spectral imager, with heritage from Ralph (Reuter et al., 2008). It consists of a single telescope that feeds two sets of focal planes: the Multispectral Visible Imaging Camera (MVIC) and the Linear Etalon Imaging Spectral Array (LEISA), which are pushbroom instruments.

## 6.4 Lander Inspection Camera

The LIC would be used to image the: landing site upon descent and surface after touchdown. It is derived from the Rosetta Lander Imaging System (ROLIS) on the Philae Lander (Mottola et al., 2007). During the landing phase, LIC would acquire images of the landing site with increasing spatial resolution. After landing, LIC would image the surface beneath the lander to provide high-resolution images of the surface, providing critical information on surface texture and various ice/regolith features such as cracks, vents, pores, sublimation features, ice grains, and mineral deposits. It has four arrays of monochromatic light-emitting diodes that operate at 470, 530, 640, and 870 nm, enabling multispectral imaging.

## 6.5 Air and Ground Temperature Sensors

Temperature sensors would be used to:

1) Determine ground and air temperature.
2) Provide contextual information for the *in-situ* measurements made on the lander.

The AGTS consists of two pairs of the temperature sensors, placed diagonally on the lander. The sensors are protected by an inhouse calibration unit containing a heating plate and a PT1000 sensor coupled to the pyrometer mounting plate, similar to the system on the Rover Environmental Monitoring Station (REMS) on Curiosity (Sebastián et al., 2010; Gómez-Elvira et al., 2012). This calibration unit helps protect the sensors from contamination from the plume eruptions. Ground temperature is recorded with a thermopile that views the surface through a filter with a bandpass of 8–14 microns and air temperature is recorded with the PT1000 sensor that is placed on a small rod that keeps the sensor outside

of the instrument's mast and boom thermal boundary layers (Gómez-Elvira et al., 2012).

## 6.6 Radio Science Experiment

The RSE would be used to characterize the:

1) Gravity field of Enceladus.
2) Tidal love numbers.
3) Topography of the oceanic floor.

The primary science objective of RSE is to constrain geophysical parameters of Enceladus by means of radiometric tracking techniques. Understanding the interior structure of the body provides insight into the spatial extent of geochemical interactions (Vance et al., 2018; Mackenzie et al., 2020), such as interface area for water-rock interactions (Dombard and Sessa, 2019). Additionally, RSE would be used to provide insight how tidal dissipation is distributed between the core, ocean, and ice shell. Measuring the tidal Love number $k_2$ would allow a determination of the tidal phase lag and total tidal dissipation (Ermakov et al., 2021). The Love numbers are used to describe how the gravity field and shape of Enceladus respond to time-varying tidal forces (Ermakov et al., 2021). Future gravity-focused missions could continue to improve constraints on Love numbers such that tidal heat generation could be constrained (Ermakov et al., 2021).

RSE gravity field measurements coupled with topography derived from Cassini (Nimmo et al., 2011; Tajeddine et al., 2017) and higher-resolution local OICAM stereo images (Park et al., 2020) would be used to constrain the internal density structure, seafloor topography (Koh et al., 2022), and ice shell degree of compensation (Ermakov et al., 2021). Additionally, crosslink observations collected during the lander descent would help resolve deviations in the local gravity field around the SPT.

The RSE, derived from Cassini Radio Science (Kliore et al., 2004), can operate in one-way downlink and coherent two-way modes. In two-way mode, a stable frequency reference at a Deep Space Network (DSN) station facility is used to generate a microwave carrier waveform. The reference oscillator aboard ETNA is disciplined using the incoming reference signal. The high-gain feed off the onboard transponder is used to coherently retransmit the carrier wave back to Earth. Radio-tracking would commence several hours prior to the periapsis and conclude a few hours after. The data collected at the beginning and end of the interval would help establish a baseline for the phase-noise variance in the frequency residuals. Collocated observations by the OICAM prior and posterior to the pass would improve uncertainty of the estimates by constraining the relative dynamics.

## 6.7 Distributed Seismic geopHOning Oceans and Crusts network

The final scientific package included in the ETNA payload is the SHOOC network, which would be used to study the physical structure, dynamics, and bulk properties of Enceladus. Monitoring the seismic activity of Enceladus would provide critical information on the structure and dynamics of its core, ocean, and crust (Panning and Romanowicz, 2006; Vance et al., 2018, 2021). It would also provide information on the dynamics of the plume systems that connect the subsurface ocean to the planet's surface boundary. Variations in thermal stress and local pressure affect the water-rock interactions, which can ultimately produce chemical disequilibria in the system (Vance et al., 2016; MacKenzie et al., 2020, 2021). Detailed seismic measurements could also enable the identification of bubble collapses in the subsurface hydrothermal venting system (Dawson et al., 2012), which may transport macromolecule organics (Postberg et al., 2018).

The SHOOC network includes three deployable probes that have low-distortion miniature geophones with a bandwidth capability of 0.1–240 Hz to capture seismic waves propagating through Enceladus (Hou et al., 2021). Each probe also has a temperature-sensing element embedded along the exterior of the telescopic mast to measure the vertical profile of the temperature, and a Micro-Electro-Mechanical Systems Inertial Measurement Unit (MEMS IMU) to measure the direction of the gravity vector (Hou et al., 2021). The SHOOC probes have two operating modes: passive mode and active mode, at which time an impactor is delivered from the orbiter to the surface of Enceladus close to the Tiger stripes to create a localized, high-frequency seismic shock (Section 8.3). Daily seismograms with minute-resolution would be collected to analyze background and induced seismic noise in the passive and active modes, respectively. In active mode, the geophones would be used to measure P-waves and secondary waves resulting from the kinetic impactor. These data would be used to analyzed temporal and spatial variations of the crustal elastic properties, for example related to vent activity (Wu et al., 2020). Geophone data from active seismic experiments during the Apollo mission have been used to analyze S-wave travel times using wavefield gradient analysis (Sollberger et al., 2016) and P-wave arrival times to create multi-layer seismic velocity models for the lunar interior to depth of ~1000 km (Heffels et al., 2017, 2021).

The distributed SHOOC network was designed as a direct response to the CSC mandate of including multiple landed elements. It is the only component of the ETNA mission with a low TRL (estimated at three in 2019), but it was designed to utilize space-grade, commercial, off-the-shelf components, similar to seismic packages that have been deployed in terrestrial glacier sites (Jones and Gudmundsson, 2013). Many design elements have heritage from the Asteroid Geophysical Explorer (AGEX) proposed to study Didymos (Karatekin et al., 2016) and LUNAR-A developed for the Moon (Mizutani, 1995; Mizutani

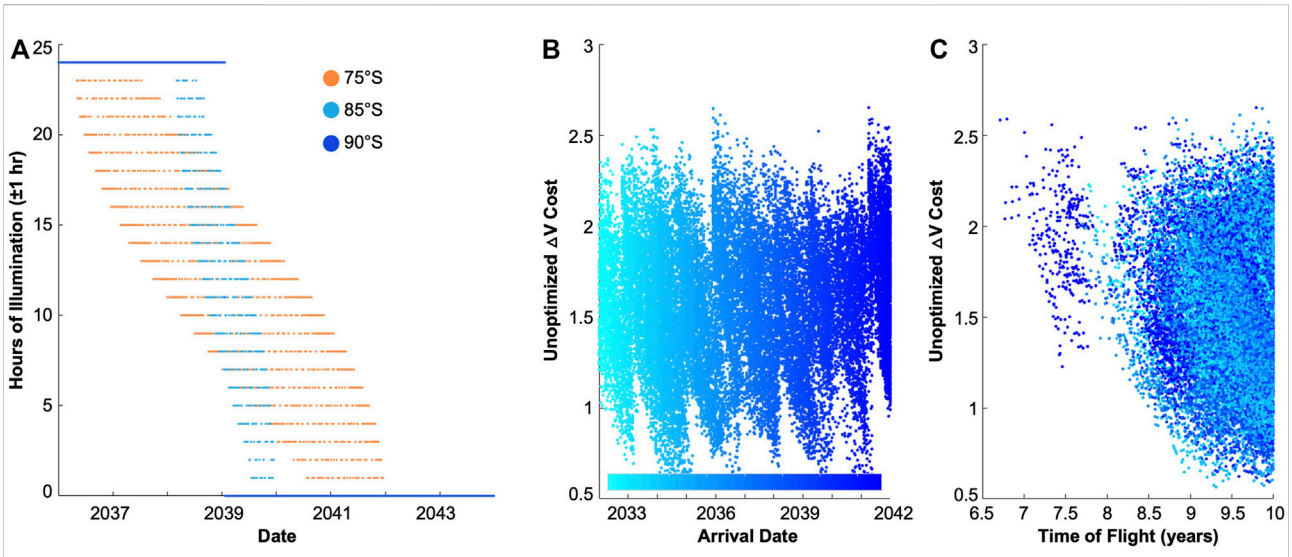


FIGURE 4
**(A)** Hours of illumination on the surface of Enceladus for each Earth day. ΔV as a function of **(B)** arrival date and **(C)** time of flight for the interplanetary transfer. The colormap labels the arrival date for the different unoptimized ΔV cost. The same colormap is used to analyze the same results in terms of time of flight to evaluate the time of departure.

et al., 1995). Under the framework of a New Frontiers mission, we would propose to include the network as a technology demonstration, given that the SHOOC's relatively low-TRL components are associated with higher risk. Achieving threshold science does not rely on the SHOOC network (Figure 2), but the scientific return of ETNA would be substantially enhanced by the network.

## 7 Mission analysis and concept of operations

To fulfill the scientific objectives presented in our Science Traceability Matrix (Figure 2), the ETNA spacecraft is composed of three segments: the orbiter, the lander, and deployable SHOOC distributed probes. In this section, we present the mission profile, mission phases, and conops. Detailed descriptions of each subsegment are presented next, in Section 8. Details on mission and implementation risk assessments in accordance with guidelines from NASA's Independent Verification and Validation program (Northey and Kinney, 2014) and pathways to mitigate and minimize these risks are in the Supplementary Information.

### 7.1 Launch, interplanetary cruise, and Enceladus arrival

The Saturnian system is a difficult target to reach because of its far distance from Earth, requiring long flight durations and the need for multiple flybys to reduce overall fuel cost. The main driver for the transfer design from Earth to Enceladus is that its south pole will enter a long period of shadow beginning in 2039 (Figure 4A). The absence of illumination limits the optical camera in the visible channels (although no other scientific instruments on the ETNA payload) and could hinder placing the various geochemical, geophysical, and biological measurements into a broad geologic context.

This includes using innovative Titan Aerogravity Assist maneuvers (Hajdik et al., 2020). As discussed in detail in the Supplementary Information, a gravity assist by Titan is associated with potential contamination by organics in Titan's atmosphere, which could compromise astrobiological measurements of Enceladus. Thus, the Titan gravity assist is used here strictly as a means to calculate approximate cruise and arrival times and ΔV costs, but we would require the selection of alternative Enceladus-approaches prior to our mission.

By considering interplanetary trajectories and orbital insertions, an arrival date at Enceladus can be set, thereby backdictating the required departure date and associated ΔV costs. Figures 4B,C provide a representation of available interplanetary trajectories from Earth to the Saturnian system in terms of ΔV (proportional to fuel use), arrival date, and time of flight, considering trajectories with flight times <10 years.

We concluded ETNA could launch on an SLS-type rocket on 2 March 2028 to arrive at Saturn on 23 June 2037, requiring a C3 of 20.97 $km^2/s^2$. The interplanetary gravity assist trajectory would take ETNA from Earth to two sequential Venus gravity assists, a Mars gravity assist, then a final Earth gravity assist before Saturn arrival. The unoptimized total ΔV for deep space

TABLE 3 Orbiter ΔV budget.

| Transfer maneuver | ΔV (km/s) |
|---|---|
| Interplanetary | 1.2 |
| Pump-Down | 3 |
| Maneuvers at Enceladus | 0.7 |
| Disposal | 0.3 |
| Total Orbiter ΔV | 5.3 |
| Total Orbiter ΔV with 5% margin | 5.6 |

maneuvers and Saturn orbit insertion is 1.088 km/s, though we use a conservative estimate of 1.2 km/s when accounting for fuel needs. This allows us to be flexible and robust to schedule changes as the unoptimized ΔV cost does not change rapidly in the vicinity of the selected trajectory (Figure 4). ETNA would take 2 years from capture into the Saturnian system to reach orbit around Enceladus on 23 June 2039.

## 7.2 Enceladus orbital operations

Orbiting Enceladus is complicated by the surrounding dynamical environment, which is strongly affected by Saturn's presence. Periodic orbits following conic sections (two-body orbits) are poor approximations in the Saturn-Enceladus system, and a baseline science orbit must be selected considering the effect of Saturn's gravity on the orbit around Enceladus (Russell and Lara, 2009). We refrained from selecting any low-altitude polar circular orbit, which is unstable around Enceladus and requires frequent station-keeping maneuvers (SKMs) (Ermakov et al., 2021). Instead, we selected an eccentric, high-inclination halo orbit with high-altitude passages at the SPT, requiring fewer SKMs and reducing the ΔV budget (Russell and Lara, 2009; Davis et al., 2018; Massarweh and Cappuccio, 2020; Ermakov et al., 2021). Specifically, we selected a L2 halo orbit designed by Davis et al. (2018) (their Figure 1) with periapsis near the south pole of Enceladus, enabling a variety of science operations to investigate the plumes. It has a periapsis altitude of ~125 km and an orbital period of 13.3 h, which ensures repeatability of observations and reasonable operation scheduling from flight dynamics teams. The orbit was approximated by a Keplerian orbit using the same periapsis and orbital period defined by Davis et al. (2018) for the sake of computing SKMs, Earth visibility, communication passages, and south polar observation time. To make the design robust to this Keplerian simplification, suitable margins were imposed on the ΔV budgets (Table 3). At this stage of the design, SKMs have been designed to occur every two orbital periods to target the orbit periapsis, which is sufficient to maintain orbit stability. This is a conservative design given that previous analyses indicate the selected orbit family is stable for more than two revolutions (Davis et al., 2018; Massarweh and Cappuccio, 2020). Future studies should investigate the SKMs in more representative dynamical models and with a detailed station-keeping strategy (e.g., MacKenzie et al., 2020).

Once at Enceladus (23 June 2039), ETNA would begin its pre-landing orbital phase (PLOP; 1 month), followed by a lander operation phase (LOP; 6 days), and a final after-landing operation phase (ALOP; 6 months; Figure 5). Nominal mission operations conclude on 9 January 2040, when latitudes poleward of 85°S are in complete shadow, although extended mission operations could continue to utilize the UVIS and RS (while OICAM will be photon-starved in the SPT). A future mission iteration could extend the mission timeline to January 2041 to maximize on the last year of dwindling illumination. Our current conops (Figure 5) prioritize landed laboratory measurements early in the mission architecture and ensures the landed laboratory is placed on the surface in illumination (Figure 4) given its vision-based landing system.

The PLOP is crucial for several reasons. It provides regional and global context for interpreting ETNA and Cassini measurements and allows for a more detailed landing site characterization (and possible adjustments). Plume fly-throughs ensure fulfillment of the Goal 2 (Figure 2) even in case of landing failure. (Note, landing is still a mission requirement and priority because the plume materials collected by the lander would be richer in complex molecules.) The PLOP also provides images of active plumes in UV-VIS wavelengths for Objs. 1B and 1C and constrains the gravity field and tidal love numbers for Obj. 1B.

The PLOP is composed of three main phases: the Imaging Campaign Phase (ICP), Spectrography Campaign Phase (SCP), and the Plume Fly-Through Phase (PFTP) commences, when ETNA flies through active plumes to collect samples for analysis by the IMAMS suite. This operation is performed before the lander release to ensure science robustness margin to the mission. The PFTP occurs at an altitude of 25 km, selected as the maximum altitude at which key astrobiologically-relevant materials are expelled to, so minimizing near-surface spacecraft risks. Various analyses suggest that spacecraft speeds of 3–10 km/s are optimal for volatizing and ionizing biomolecules (amino acids and fatty acids) in ice grains while preventing fragmentation (Klenner et al., 2020; Cable et al., 2021b; Jaramillo-Botero et al., 2021). As the fly-through trajectory is a critical parameter to ensure collection of heavier plume molecules, a dedicated strategy should be designed to reduce the periapsis of the operational orbit without exceeding the closest-approach velocity. Note that velocities are generally hundreds of meters per second in the Keplerian approximation and in the three-body problem (Fantino et al., 2020). Under Keplerian approximation, the current fly-through velocity at Enceladus' closest approach is

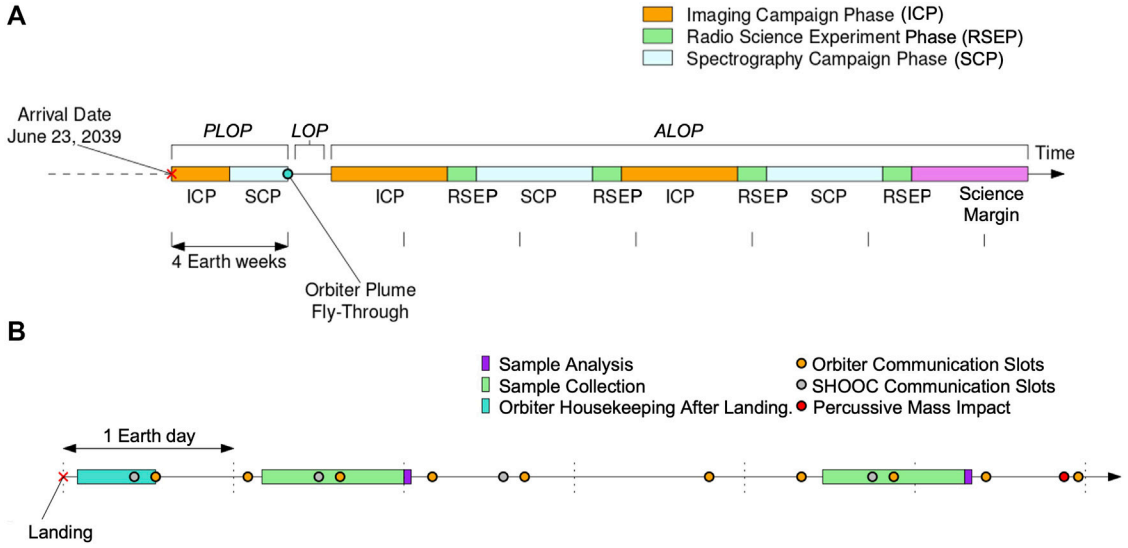


FIGURE 5
**(A)** The orbiter science operation timeline, consisting of the pre-landing operation phase (PLOP), lander operation phase (LOP), and after-landing operation phase (ALOP). The total length of orbiter operations is 29 Earth weeks, beginning on 23 June 2039 when ETNA arrives at Enceladus. **(B)** The lander sample collection timeline, consisting of an initial orbiter housekeeping phase and three sample collection (green) and analysis (purple) phases.

180 m/s. In the current mission design, the sampling altitude was computed on scientific and safety considerations without designing a detailed strategy to target the fly-through pass with the desired velocity (an order of magnitude higher).

The PLOP lasts ~ 1 month. The ICP and SCP each require 1 week to achieve complete spatial coverage of the south polar region (70–90°S). The PFTP does not place major time-scheduling constraints on the mission operations scenario, because it only requires lowering the periapsis to 25 km for < 2–5 passages, or <~1–3 days (Section 7.3.2). We apply a 100% margin to accommodate for possible inconveniences during the mapping phases that could result in losing a passage at the south pole, resulting in four total weeks of PLOP operations. The orbital period of the selected L2 halo orbit (Davis et al., 2018) would result in 56 passages at the south pole, providing sufficient redundancy for the required local mapping needs. A longer pre-landing orbital phase is not favored so that ETNA can land and commence surface operations before the surface enters a period of complete darkness, which begins 1 January 2042 at 75°S (Figure 3).

Following the PLOP, ETNA enters the LOP. Once the lander is released from the orbiter, the main task of the orbiter is to perform communication relays with the lander. It would collect data from the lander at periapsis and send it to Earth at apoapsis. After surface operations (Section 7.3), the orbiter continues with a 6-month ALOP (including a 1-month robustness margin), which is divided into three main science campaigns (Figure 5A):

1) Two post-landing ICPs (each lasting one Earth month) include imaging of the lander, deployed geophones, and science targets identified during preceding orbital operations.
2) Four dedicated Radio Science Experiment Phases (RSEPs) (each lasting 1 week) are designed for orbiter communication with the DSN to collect range and range-rate information, which bound the internal structure of Enceladus, and continued gravity field mapping.
3) Two post-landing SCPs (each lasting 1 month) include continued UV-VIS imaging of the plumes and SPT at higher spatial resolution.

Temporal separation between imaging phases (Figure 5A) would enable change-detection studies of vent morphometry and plume behavior.

## 7.3 Surface operations

### 7.3.1 Landing

Following the PLOP, the orbiter lowers its altitude closer to 150 km (shortly before the apoapsis) and releases the lander (Supplementary Figure S1). The lander then targets the final landing position and performs a soft landing in the SPT with an autonomous navigation and control system using the onboard hazard detection and avoidance algorithm (Section 8). The landing is estimated to take 30 min and use a ΔV of 400 m/s. During the landing

process, the lander deploys the three SHOOC probes sequentially to achieve ~50-m spacing (similar to the Apollo geophones; Nunn et al., 2020), as their optimal functioning requires triangulating the seismic signal. Each geophone is spun up along its axis prior to launch to give stabilization during the release and to ensure minimum position and orientation perturbation during free fall. Upon landing, SHOOC probes begin passive operations, recording "background" seismic data.

#### 7.3.2 Sample collection

Sample Collection begins when the lander arrives on the surface. The IMAMS suite requires plume samples for analysis, and our operations timeline allocates three samples for threshold science requirements. Assuming the lander is at a maximum distance of 5 km from an active plume, the required 1 µl of fresh plume materials should be collected in <20 h (Section 5.2). After sample accumulation, a cryo-motor delivers the sample to the microscope aperture for imaging. Next, the sample is halved and delivered to the two mass spectrometer subsystems (Section 6.1) and the data are relayed on the orbiter communication system and sent to Earth before a new sample is collected. The communication slots with the lander and the SHOOC probes were planned to ensure communication with the orbiter and back to Earth. This image-relay sequence was designed to be robust to lander malfunctions, and ensure critical scientific data are received prior to subsequent sampling maneuvers. After ground confirmation, the next sample collection starts, and the process is repeated. Each new sample would be collected in a clean collection slide, and the lander carries spare collection slides for safe redundancy practices. The time to collect and analyze one sample is estimated to be ~21 h, which is consistent with the orbiter orbital period. During the first passage, lander housekeeping is verified and during the second passage, scientific data are relayed (Figure 5B).

#### 7.3.3 The SHOOC science experiment

Following surface sampling and analysis, the active phase of the SHOOC science experiment starts. Up to this point in surface operations, the geophones have been passively measuring seismic signals to characterize Enceladus at low frequencies. At this point, a 56-kg percussive mass is deployed from the orbiter to impact the surface and would induce high-frequency waves to be measured by the geophones.

This experiment importantly occurs following all surface sampling and analysis to ensure IMAMS science return in case the lander affected by the percussive mass impact. A communication slot is placed right after the mass impact to ensure the lander safety with the orbiter. After this experiment, the lander remains active, imaging the surface, near-by plumes, and potential impact aftermath. Camera images are relayed to the orbiter during the remainder of the mission.

### 7.4 Orbiter disposal

The ETNA mission concept was conceived under the guidelines of NASA and the Committee on Space Research (COSPAR) Planetary Protection Policy (COSPAR, 2021), designed to prevent the forward contamination of Enceladus by Earth-based organisms, limiting probability of contamination to no more than $1x10^{-4}$ (Supplementary Material). Before launch, lander assets would be sterilized to the appropriate Category IV standards (NPR 8020.12D, Planetary Protection Provisions for Robotic Extraterrestrial Missions). The orbiter would be impacted into Saturn for disposal to avoid contact with other astrobiologically-relevant targets ($\Delta V$ ~0.3 km/s).

## 8 Spacecraft system design

### 8.1 Orbiter design

In this section, we present the different orbiter subsystems. The total orbiter dry mass is estimated to be 554.92 kg (Table 4; Supplementary Table S1).

#### 8.1.1 Structural design

The structural design of the orbiter (Figure 6) utilizes an aluminum structure supported by aluminum honeycomb carbon fiber plates for the walls. Propellant tanks are stored in the hub. The thrusters and high-gain antenna (HGA) are mounted on opposite faces of the spacecraft. OICAM and UVIS are mounted in opposition with respect to the lander to limit their degradation during the plume flythrough. IMAMS is mounted directly on the lander.

#### 8.1.2 Power

Mission power generation is limited by the low solar power flux at Saturn (15 $W/m^2$). We considered two possibilities for the power source for the orbiter: Radioisotope Thermoelectric Generators (RTGs) and solar panels. Supplementary Table S2 shows the trades evaluated for the power subsystem, which ultimately led to the selection of an RTG system due to favorable mass and power rankings and ease-of-integration. Its lowest-ranking quality is related to its potential complicating effects on planetary protection measurements, which is not a concern with solar panels. However, we found the power generation by solar panels to be infeasible under mission constraints. The large surface area required for sufficient solar panels would impose a major burden on the total spacecraft mass budget, not only for the structure, but also

TABLE 4 Overall mission mass budget, which can be managed at launch by an SLS, Delta IV, Atlas V, or Falcon Heavy at C3 = 20.97 $km^2/s^2$.

| Subsystem | Mass (kg) |
|---|---|
| 3 SHOOC probes | 48.9 |
| Lander Dry Mass (SHOOC probes excluded; See Supplementary Table S5) | 98.5 |
| Orbiter Dry Mass (See Supplementary Table S3) | 554.92 |
| ETNA Dry Mass | 702.03 |
| ETNA Dry Mass with 20% margin | 842.44 |
| Lander Mass Consumables | 36.5 |
| Orbiter Consumable | 4025.20 |
| ETNA Wet Mass | 4904.14 |

for the other subsystems given the panels' high inertia and mechanism presence (Benson, 2007). Furthermore, the solar panels would have increased the complexity during the pump down at Enceladus given the high torques the spacecraft would have experienced.

The orbiter power requirements were computed for different operating modes of the spacecraft. The maximum power consumption is the design driver for the power subsystem. It occurs during communication slots with Earth when the communication subsystem needs 100 W to ensure proper data rate with the ground station. In this phase, the attitude determination and control subsystem (ADCS) requires 60.5 W to ensure proper attitude estimation and pointing control. The onboard computer (OBC) requires 12 W ± 5 W for the attached lander housekeeping, leading to a total peak power consumption of 177.5 W. We applied a 20% margin to the peak consumption scenario to select the number of RTGs.

ETNA uses Multi-Mission Radioisotope Thermoelectric Generators (MMRTGs), which provide 110 W and 72 W at beginning- and end-of-life (BOL; EOL), respectively (Woerner et al., 2013). This design has heritage from Cassini, which carried a 885-W RTG system Cassini

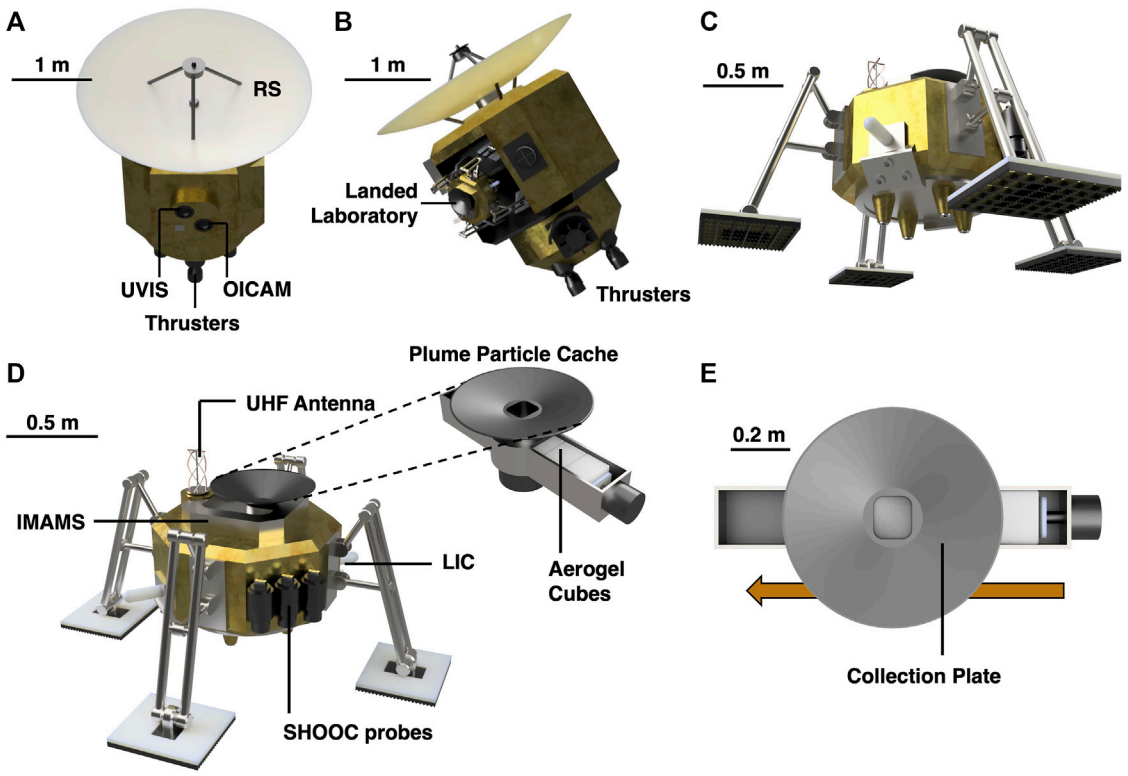


FIGURE 6
Artist's rendition of the ETNA spacecraft. **(A)** Lateral view of the orbiter where the UVIS, OICAM, and RS instruments are visible. **(B)** Lateral view of the orbiter where the lander attached is visible. **(C)** A view of the ETNA landed laboratory, highlighting the lander feet design, showing the wide surface areas and teeth. **(D)** View of the lander structural design shows the IMAMS package, UHF antenna, and Plume Particle Cache all fixed on top of the lander, as well as the LIC and deployable SHOOC probes attached to the lander sides. Dashed lines show close-up view of the Particle Cache, including the aerogel cubes. **(E)** Top-down view of the sampling collection plate on the Plume Particle Cache. Aerogel cubes are exposed one at a time and pushed through to the spectrometer. For scale, RS dish in **(A,B)** is 3 m across and particle cache in **(C–E)** is 40 cm across. Note that the fuel tanks are not included in this artist's rendition but are considered to be spherical at the present design stage (radii = 0.41, 0.56, and 0.71 m; Section 8.1.7).

(Henry, 2003; Woerner, 2017). The mass and power designs of the RTGs are deduced from the more recent design for the Mars Curiosity Rover, which has a 45-kg RTG with 70 W at EOL (Bechtel, 2013). By considering Mars Curiosity RTG characteristics, we selected a RTG that is three times more massive (135 kg) and produces three times the power at EOL (210 W). Note that more light and compact design are currently under study (Woerner, 2017) as we consider our current mass budget to be conservative. The power subsystem includes batteries that ensure 24 h of energy at 213 W consumption (i.e., the upper endmember power consumption scenario plus 20% margin). Using the NASA Europa Clipper Li-CFx batteries as a base for estimate (350 Wh/kg energy-to-mass ratio), and by considering a power margin of 20% (Surampudi et al., 2018), then the battery pack mass for the ETNA orbiter is estimated to be 15 kg. This ensures downlink of science data and communication with the ground in case of MMRTGs malfunctions. It is worth noting that a battery pack was not included in Cassini's design (Henry, 2003) but included on ETNA for power margin to downlink data in the case of unexpected fatal RTG malfunctions.

### 8.1.3 Attitude determination and control

The spacecraft ADCS was designed to be versatile for all mission phases, composed of 12 coarse Sun sensors that prevent the cameras from being pointed at the Sun one inertial measurement unit (IMU), two star trackers to calibrate the IMU and to ensure inertial pointing, one navigation camera to support flyby operations and Enceladus insertion, four reaction wheels in pyramidal configuration, and 16 1-N hydrazine thrusters to ensure pointing and wheel desaturation. This design has heritage from the Cassini spacecraft (Lee and Burk, 2019) and all the selected components have high TRLs between seven and 9.

### 8.1.4 Communication

The orbiter communication subsystem operates at X-band (8–10 GHz; Bruder et al., 2003) for nominal two-way communications, two-way tracking for doppler and ranging measurements (Thornton and Border, 2003), and changes in differential one-way ranging (DOR) (James et al., 2009), which is always performed in one-way mode. It also includes a Ka-band (27–40 GHz; Bruder et al., 2003) two-way carrier tracking capability for gravity science. The communication system is composed of a 3-m, 100-kg HGA with heritage from Cassini (Taylor et al., 2002). The HGA ensures a data rate of 1.66 Mbps with the 70-m DSN antenna by using the ESA MPTS (Multi Purpose Tracking System) ranging. Moreover, the system ensures a minimum telemetry of 1000 kbps into a 34-m DSN ground station with ESA MTPS ranging. Note that minimum telemetry needs are computed for the least favorable atmospheric and geometrical conditions for the link budget. If the spacecraft enters a safe mode, the communication is ensured with a low-gain antenna (LGA) that has a data rate is 7 bps for commands and 10 bps for telemetry with the 70-m DSN antenna. During critical events, such as main engine burns, the communication link is ensured with the LGA in downlink only. Communications with the lander are performed in UHF-band (0.3–3 GHz; Bruder et al., 2003) using a quadrifilar helicoidal antenna that supports two Mbps links.

### 8.1.5 Onboard data handling

The spacecraft's computer is a CREOLE ASIC developed by RUAG Space with a TRL of 9. For redundancy and risk mitigation, two OBCs are included. The CREOLE ASIC has two 374-Gbit memories with Error Detection And Correction (EDAC), making the design robust to high data volumes. The spacecraft also has a NAND Flash Module-DDC with 196-Gbit memory, which allows for several Enceladus orbits and data collection events without the need for direct downlink to Earth, as the highest-volume data segments are 15 Gbits (acquired during a measurement pass from OICAM). Thus, all OICAM mapping could be performed without downlink to Earth. Future work is needed to refine total data volume estimates for each of the operational phases and to schedule data downlink operations.

Considering the low radiative environment of Saturn, latch-up and single event upsets (i.e., events from particles impacting the electronics that cause hardware damage) should not be a major issue for the OBC, given the radiation hardening of the selected components.

### 8.1.6 Thermal

The thermal control system was designed to minimize the influence of the external environment on the spacecraft, withstanding both harsh high temperatures from solar heating during inner planet flybys, and also harsh cold temperatures in the Saturnian system. At Enceladus, some of ETNA's external surfaces would experience temperatures < −200°C, with even colder conditions during solar eclipses when the spacecraft is in Saturn's shadow. For the ETNA mission, the operating Allowable Flight Temperature (AFT) limits are −20–40°C and the non-operating AFT limits are −40–70°C.

To protect the spacecraft and its components from the thermal environment, high eficiency Multi-Layer Insulation (MLI) and General Purpose Heat Source (GPHS) modules from the MMRTG are used. The MLI material selected to blanket the spacecraft's exterior is the StaMet coated black kapton 160XC (Avila et al., 1998). The MLI moderates the external temperature during the spacecraft's closest approach to the Sun. The HGA could also be used as a thermal shield, as it was for Cassini (Fabiani and Costabile, 1997). The MLI must also limit heat leakage to minimize power demand from the

spacecraft's heaters, especially when instruments are operating during science and communication phases. The thermal subsystem requires internal heat generation to fulfill the operating and non-operating AFT requirements. Mars Curiosity's MMRTG is composed of 8-GPHS modules (Woerner et al., 2013), which can provide up to 250 W of heat power per module. As the orbiter has a MMRTG which generates three times more power (Section 8.1.2), we estimate that enough heat power is generated by the MMRTG. The obiter takes advantage of this heat, which is a by-product of the nuclear energy generation, to comply with ETNA temperature requirements. Thus, no other RTG is considered for the thermal generation and the power system heat by-product is used to fulfill temperature requirements. The heat is distributed with heat pipes to critical subsystems.

We calculated temperatures of the hub interior and orbiter exterior faces for "cold" and "hot" cases, both with and without MMRTG thermal power (Supplementary Table S3). More detailed analysis is needed to understand if the MMRTGs can be exploited to ensure the correct orbiter heating without the need of other heat sources.

### 8.1.7 Propulsion

The propulsion system for the orbiter uses a hypergolic bipropellant system with hydrazine for fuel, mixed oxides of nitrogen (MON) for the oxidizer, and helium pressurant. The main engine is the LEROS 1b, which provides 635 N of thrust at a specific impulse of 320 s and an oxidizer-fuel ratio of 1.65. The orbiter is also equipped with 16 reaction-control system (RCS) throttleable engines, which are 1-N hydrazine thrusters that operate at a specific impulse of 230 s. These RCS engines use hydrazine in a monopropellant configuration. Both engines have strong flight heritage, including use on NASA's Juno mission to Jupiter (Stephens, 2015).

The system is budgeted to perform all orbital maneuvers presented in Section 7. This corresponds to 1519.08 kg of hydrazine and 2506.48 kg of MON stored in spherical carbon fiber overwrap tanks with radii of 0.71 m and 0.56 m, respectively. This provides an ullage of 5% of the total volume when completely filled. The tanks are pressurized to 1.54 MPa with inert helium gas that is stored in a separate composite overwrapped pressure vessel with a radius of 0.41 m. ETNA includes a 65-kg pump assembly like that on Cassini (Leeds et al., 1996) to ensure the correct distribution and pressurization within the subsystem.

## 8.2 Lander design

The landed laboratory includes the IMAMS suite, temperature sensors, a series of cameras for landing and scientific investigation purposes, including the LIC, and the deployable SHOOC network (Figure 6). The design of the landed laboratory was heavily influenced by the needs for 1) power generation for at least seven Earth days and 2) soft autonomous landing in potentially porous terrains. In this section, we describe the different subsystems. The total lander dry mass excluding the SHOOC probes is estimated to 95.5 kg (Table 4; Supplementary Table S4).

### 8.2.1 Structural design

The lander structure is an aluminum chassis with aluminum honeycomb carbon fiber side panels. The outermost layer is surrounded with Mylar for radiative heat transfer control. The landing legs are derived from the Europa Lander concept (Dooley, 2018), and allows for landing in a diverse set of ground conditions (e.g., hard ice, regolith, unconsolidated icy materials). The lander hub is raised above the ground, minimizing the risk of instrumentation being damaged by the environment during landing. The feet of the lander have large surface areas to provide stability and prevent sinking into the snow on the surface. The sole of each lander foot has teeth to prevent slippage in case of landing on uneven ground (Figure 6C).

### 8.2.2 Power

The landed laboratory necessitates operation of the spacecraft for at least seven Earth days, while *in-situ* scientific analyses are conducted on the laboratory and data are communicated back to the orbiter, which then relays the data back to Earth. We considered three different options while exploring the trade space for potential power sources: RTGs, solar panels, and batteries (Supplementary Table S5). As with the orbiter power design (Section 8.1.2), solar panels are unfavorable due to unfavorable mass, power, and operational lifetime properties. RTGs offer desirable power generation, heat generation, and operation length, but are associated with high costs of planetary protection requirements. A protective shell around the RTG may help prevent potential contamination (Konstantinidis et al., 2015). Moreover, recent work on the Orbilander study (MacKenzie et al., 2020, 2021) suggests that RTG heat is unlikely to melt ice crusts with surface temperatures <85 K and alter subsurface ocean chemistry. Nevertheless, given the criticality of planetary protection in an astrobiology mission, we selected to use a battery pack based on the studies performed for the Europa Lander mission (Dooley, 2018; Hand et al., 2022). These batteries can last for several days and have high energy-to-mass ratios (>700 Wh/kg), which make them suitable for outer planet exploration (Dooley, 2018; Bugga and Brandon, 2020). The power need of the lander (excluding the thermal subsystem) is 2978.8 Wh with 20% margin for 1 week of operations

TABLE 5 Power budget for the lander. The lander operates the GNC and propulsion system during the descent and landing phase of 30 min. Lander instruments analyze the collected sample over a period of 1 h during the sample analysis phase. The communication system communicates for 1 h with the orbiter during the communication phase which happens every orbiter passage (every 13.3 h). The onboard computer works continuously for the overall lander operations in all phases.

| Subsystem | Power (W) | Nominal active time during operation phase (hrs) | Phase | Energy (Wh) | Energy with 20% margin (Wh) |
|---|---|---|---|---|---|
| Instruments | 90 | 1 | Sample Analysis | 90[a] | 108 |
| GNC | 74 | 0.5 | Landing | 37 | 44.4 |
| Propulsion | 14 | 0.5 | Landing | 7 | 8.4 |
| Communication | 30 | 1 | Comm | 30[b] | 36 |
| Onboard Computer (Data Handling) | 10 | Continuous | All | 1680 | 2016 |

[a]Per sampling (3 total).
[b]Per communication slot (16 total).

(Table 5). Assuming 90 W are needed continuously for the thermal subsystem to power a resistive heater (Section 8.2.6), the total energy to be stored in the batteries is 18,098.7 Wh. This energy is stored in a 27-kg Li/CF battery pack that provides up to 18,900 Wh.

### 8.2.3 Attitude and orbit determination and control

Although nominal landing is expected to occur during illumination, there will still be regions of shadow. The GNC suite includes a visual camera and flash LiDAR mounted on the lander belly that enable landing in poorly (or non-) illuminated regions. The flash LiDAR has heritage from the OSIRIS-REx mission (Sornsin et al., 2019), has shown compelling performances from 3 km to 0.3 m of altitude, and can support autonomous pinpoint landing (Kanani et al., 2016). The landing phase is ensured by the camera and IMU fusion by image-processing techniques based on feature tracking on Enceladus' surface (Duteïs et al., 2019). Verification and validation studies using synthetic measurements from high-fidelity rendering engines (e.g., Lebreton et al., 2021) and hardware-in-the-loop tests (Duteïs et al., 2019) would occur pre-launch. The control system is composed of a hydrazine-based reaction control system that can damp the lander oscillation due to the thruster misfiring and orient the lander correctly during the descent.

### 8.2.4 Communication

The lander communication subsystem is composed of an Iris transponder in UHF band with a medium-gain antenna. It operates at UHF-band for two-way communications (command and telemetry) and for data relay from lander to spacecraft. The link budget is designed to handle the highest-data-volume communication uplink, which occurs after IMAMS sample analysis (~1.6 Gbits of data). The other visibility windows are used for relay of the SHOOC probes and housekeeping information.

### 8.2.5 Onboard data handling

When the lander is not in visibility for communication with the lander, the data is stored in a 196-Gbit NAND Flash Module-DDC. The high onboard data storage capability ensures sufficient memory even with several lost communication passages. The onboard data handling is managed by two LEON 3FT onboard board computers, one for redundancy, chosen for their flight-proven reliability and high TRL of 9.

### 8.2.6 Thermal

The lander faces challenging thermal conditions on the surface of Enceladus. The four lander legs minimize conductive heat loss to the environment by limiting the heat path from the instrumentation and avionics to the surface. Despite this design, the lander requires active heating throughout the entire mission to fulfill operative and non-operative AFT requirements.

Lander power consumption provides 90 W of heat power from resistive heaters over the course of landed operations. The battery pack produces an additional 90 W of heat power (1 W of heat power for every watt of electrical power; Schmidt and Bhandari, 2019), without considering other energy consumptions due to operations. Thus, at least 180 W of heat power are available to heat the lander during its operative life. Coupled with heat pipes and insulation, this heat power can be used to fulfill temperature requirements, as in the Europa Lander study (Schmidt and Bhandari, 2019). Note that further analyses are required to size the power and thermal subsystems for an optimized solution. Our current design includes battery packs placed around the lander hub, similar to the Europa Lander.

### 8.2.7 Propulsion

The lander was designed to handle a soft autonomous landing. To ensure safe and accurate delivery of the lander,

TABLE 6 Power and mass budget for a single SHOOC probe (note: ETNA includes three). The probe sensor suites and OBCs continuously operate for seven Earth days. The communication system communicates with the lander for 30 min every 24 h.

| | Geophones | IMU | Temperature sensors | Communication | Onboard data handling | Telescopic tubular mast | Storable tubular extendible member | Battery |
|---|---|---|---|---|---|---|---|---|
| Number | 1 | 1 | 2 | 1 | 1 | 1 | 1 | 1 |
| Power (W) | 0.4 | 0.4 | 0.2 | 15 | 0.2 | -- | -- | -- |
| Duration (hrs) | 24 | 24 | 24 | 0.5 | 24 | -- | -- | -- |
| Repetition | 7 | 7 | 7 | 7 | 7 | -- | -- | -- |
| Energy (Wh) | 67.2 | 67.2 | 67.2 | 52.5 | 33.6 | -- | -- | -- |
| Mass (kg) | 0.1 | 0.054 | 0.1 | 0.065 | 0.1 | 6 | 9 | 2 |

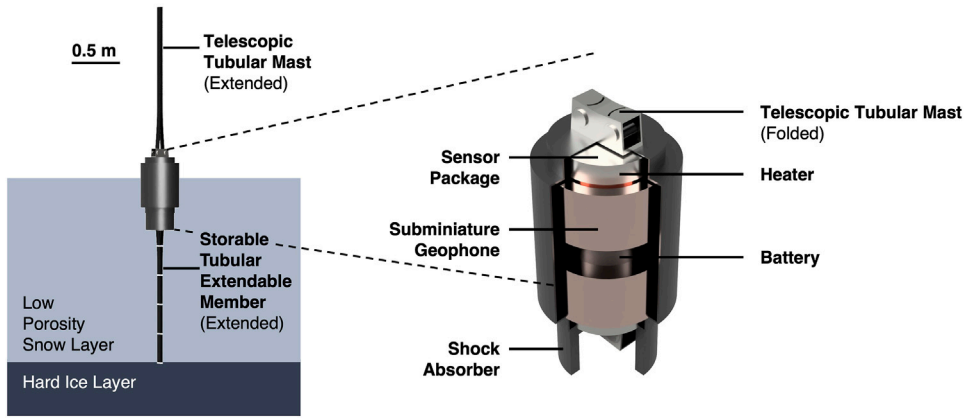


FIGURE 7
Artist's rendition of the SHOOC system. The schematic illustrates a SHOOC probe embedded on the surface of Enceladus, with both telescopic components deployed. A zoom-in shows the Interior cross-section diagram of a probe. For scale, tubular masts are 1.5 m long.

powered landing would be implemented on the spacecraft. The lander's propulsion system is a monopropellant system using hydrazine and pressurized with helium. The propulsion system consists of four monopropellant engines capable of individually throttling between 1.3 and 5.3 N, giving the lander the capability to deorbit, descend, and land. The engines have flight heritage from their use as trajectory correction engines for the Mars Science Laboratory (Weiss and Guernsey, 2013).

The four engines are statically attached to the central hub and directed toward the landing surface since attitude control is managed by the reaction wheels. Each engine consumes hydrazine at a rate of 0.6–2.4 g/s and operates with a specific impulse of 230 s. The lander is capable of soft landing with two engines in case of engine failure. The total consumable, including the RCS required mass, is 36.5 kg, which is stored in a single shared tank on the lander. A separate helium tank provides the necessary 28-bar feed pressure.

## 8.3 SHOOC system design

The SHOOC system is a custom-designed, distributed network enabling seismic investigations of Encealdus' interior. It includes a percussive mass carried by the orbiter and three deployable 16.3-kg probes (Tables 4, 6) carried by the lander that are dispersed during the landing sequence.

As discussed in Section 6.7, the SHOOC system works first in passive mode (measuring background ground movements) and then in active mode, which begins when a percussive 56-kg metallic mass is released from the orbiter at 125-km altitude, creating a local seismic shock on the surface nearby the probes. The impactor would be composed of distinct materials that, if disrupted, could be uniquely identified from materials native to Enceladus.

Each probe has a sensor package with temperature sensors and a miniaturized geophone that detects acoustic signals and stores them in local internal memory on data handling subsystems. The geophones are custom designed to enable direct contact with the ground for seismic monitoring (the IMU system can tell when ground contact is made using an onboard accelerometer).

A shock absorber is located at the bottom of each probe, designed to crumple and prevent bouncing or damage to the probe. If the ground is covered in soft snow, the probe would burrow itself into it, and if the ground is hard ice, the shock absorber would take the impact of the landing.

Once a probe lands, it extends its storable, tubular member until contact is made with a consolidated surface (Figure 7), or until the tubular member extends to its full length. Extending the member improves the signal-to-noise ratio by decreasing the seismic dampening that a snow layer may have. Next, a 1.5-m telescopic tubular mast is deployed from the top end of the probe. This mast mounts on top of an antenna and its purpose is to clear the surface to allow communication with the lander in UHF, even in conditions where the probe becomes covered by deposited plume materials or sinks into a low-porosity, snowy surface layer.

Temperature control is managed with an insulating aerogel layer and an internal resistive heater. The aerogel was selected for its low thermal conductivity (~0.01 W/mK; Jones and Sakamotot, 2006) that could lead to low-power resistive heater. The current design does not account for a detailed thermal analysis, and we estimated that a 1-kg battery is sufficient to power the heater system during SHOOC operations. Detailed studies should be performed in future work to understand the required power for the heating system, to optimize the thickness of the aerogel insulation, and to prove the feasibility of the proposed combination of low-power heater and aerogel insulation and its compliance to the 1-W requirement.

The three SHOOC probes operate independently and continuously for a minimum of seven Earth days. Each probe hosts a communication subsystem that communicates with the lander for 30 min every 24 h, resulting in a total power budget of 345.24 Wh, which includes a 20% margin (Table 6). Utilizing the same batteries as those on the lander, a 2-kg battery pack is included with each SHOOC probe, sufficient for power subsystem needs.

Considering that the lander releases the probes during its descent trajectory, the maximum distance between the lander and the probes is conservatively estimated to be 45 km for the communication design is 45 km. The communication system of each SHOOC probe can manage up to 450 Mbits of data per Earth day, to be sent to the lander *via* UHF-band one-way link. The communication system works at 400 MHz and can send >1 Gbits of data in 30 min, which is more than sufficient to send scientific and housekeeping data of the probe.

# 9 Conclusion

The ETNA mission concept provides an Enceladus exploration architecture as a means of better understanding the origin and evolution of habitability and life in our Solar System through a combination of orbital observations, plume fly-throughs, and landed sample analyses. The next phase of transformational Enceladus science must extend beyond assessing the habitability of the moon, given that Cassini has demonstrated a baseline of habitability with the coincident presence of liquid water, the necessary chemical ingredients for life as we know it (e.g., hydrocarbons, organics, salts, and nitriles), and an energy source (water-rock interactions). The next investment in Enceladus science should focus on signs of life (*What biotic signatures characterize Enceladus?*) and processes (*Does Enceladus provide habitable conditions?*). An Enceladus mission that is focused heavily on astrobiology (*Is or was the moon ever inhabited?*) will provide the greatest new return on Solar System science, and such a mission likely extends beyond a New Frontiers-class architecture into a Flagship-class architecture. This is synergistic with the strategy outlined by the recently released Origins, Worlds, and Life: A Decadal Strategy for Planetary Science and Astrobiology 2023–2032 (NRC, 2022), which prioritizes astrobiology science investigations of Enceladus using a combined orbiter-lander approach.

# Data availability statement

The original contributions presented in the study are included in the article/Supplementary Material, further inquiries can be directed to the corresponding author.

# Author contributions

All authors contributed equally to the conception and design of the ETNA mission, and the creation of a final study report that was presented at the Caltech Space Challenge and served as the preliminary version of this paper. AND and PP iterated on the design and wrote this paper. LT-O, VDP, YHC, CV, and TM provided critical feedback and writing support.

## Funding

The contributing authors are/were all students who participated in the fifth Caltech Space Challenge, which was sponsored and supported by Lockheed Martin, Keck Institute for Space Sciences, Northrop Grumman, Aerospace Corporation, NASA's Jet Propulsion Laboratory, GALcit, the Moore-Hufstedler Fund, and Caltech.

## Acknowledgments

We gratefully acknowledge helpful reviews by Francis Nimmo and an reviewer. We are very thankful to the following persons for their mentorship and support: S. Toedtli, F. Royer, N. Angold, M. Cable, D. Landau, T. Nordheim, J.-P. de la Croix, J. Karras, G. Meiron-Grith, T. Heinsheimer, D. Murrow, and JPL's A-Team. We also thank the spirited participants of Team Voyager, who participated in the 2019 CSC as well: K. Valachandran, P. Cappuccio, J. Di, K. Doerksen, J. Fuchs, A. Gloder, R. Jolitz, M. Li, D. Limonchik, L. Massarweh, A. Meszaros, D. Naftalovich, E. Nathan, T. Peev, M. Rovira Navarro, and S. Santra. This mission design would not have been possible without the support and funding of Lockheed Martin, Keck Institute for Space Sciences, Northrop Grumman, Aerospace Corporation, NASA's Jet Propulsion Laboratory, GALcit, the Moore-Hufstedler Fund, and Caltech.

## Conflict of interest

The authors declare that the research was conducted in the absence of any commercial or financial relationships that could be construed as a potential conflict of interest.

## Publisher's note

All claims expressed in this article are solely those of the authors and do not necessarily represent those of their affiliated organizations, or those of the publisher, the editors and the reviewers. Any product that may be evaluated in this article, or claim that may be made by its manufacturer, is not guaranteed or endorsed by the publisher.

## Supplementary material

The Supplementary Material for this article can be found online at: https://www.frontiersin.org/articles/10.3389/fspas.2022.1028357/full#supplementary-material.

## References

Arevalo, R., Ni, Z., and Danell, R. M. (2020). Mass spectrometry and planetary exploration: A brief review and future projection. *J. Mass Spectrom.* 55, e4454. doi:10.1002/jms.4454

Arevalo, R., Selliez, L., Briois, C., Carrasco, N., Thirkell, L., Cherville, B., et al. (2018). An Orbitrap-based laser desorption/ablation mass spectrometer designed for spaceflight. *Rapid Commun. Mass Spectrom.* 32, 1875–1886. doi:10.1002/rcm.8244

Avila, A., Rouse, N., Clark, S., Tsuyuki, G., and Millard, J. (1998). *A summary of the Cassini spacecraft thermal performance from launch through early cruise*. Pasadena: JPL California Institute of Technology.

Barge, L. M., and Rodriguez, L. E. (2021). Life on Enceladus? It depends on its origin. *Nat. Astron.* 5, 740–741. doi:10.1038/s41550-021-01382-4

Bechtel, R. (2013). *Multi-mission Radioisotope thermoelectric generator*. Availableat: https://www.nasa.gov/sites/default/files/files/4_Mars_2020_MMRTG.pdf.

Běhounková, M., Souček, O., Hron, J., and Čadek, O. (2017). Plume activity and tidal deformation on Enceladus influenced by faults and variable ice shell thickness. *Astrobiology* 17, 941–954. doi:10.1089/ast.2016.1629

Benson, S. W. (2007). "Solar power for outer planets study," in *Outer planets assessment group (OPAG)* (Greenbelt, MD: OPAG Meeting).

Beuthe, M., Rivoldini, A., and Trinh, A. (2016). Enceladus's and Dione's floating ice shells supported by minimum stress isostasy. *Geophys. Res. Lett.* 43 (10), 10,088–10,096. doi:10.1002/2016GL070650

Bibring, J.-P., Lamy, P., Langevin, Y., Soufflot, A., Berthé, M., Borg, J., et al. (2007). *Space Sci. Rev.* 128, 397–412. doi:10.1007/s11214-006-9135-5

Bretscher, M. S. (1985). The molecules of the cell membrane. *Sci. Am.* 253, 100–108. doi:10.1038/scientificamerican1085-100

Brown, R. H., Clark, R. N., Buratti, B. J., Cruikshank, D. P., Barnes, J. W., Mastrapa, R. M. E., et al. (2006). Composition and physical properties of Enceladus' surface. *Science* 311, 1425–1428. doi:10.1126/science.1121031

Bruder, J., Carlo, J., Gurney, J., and Gorman, J. (2003). *IEEE standard for letter designations for radar-frequency bands*. IEEE Aerospace & Electronic Systems Society, 1–3.

Bugga, R. V., and Brandon, E. J. (2020). Energy storage for the next generation of robotic space exploration. *Electrochem. Soc. Interface* 29, 59–63. doi:10.1149/2.F08201IF

Bywaters, K., Stoker, C. R., Batista Do Nascimento, N., and Lemke, L. (2020). Towards determining biosignature retention in icy world plumes. *Life* 10, 40. doi:10.3390/life10040040

Cable, M., MacKenzie, S., Neveu, M., Hoehler, T. M., Hendrix, A. R., Eigenbrode, J., et al. (2021a). The case for a return to Enceladus. *Bull. AAS* 53. doi:10.3847/25c2cfeb.2a04ec49

Cable, M., Waller, S. E., Hodyss, R., Hofmann, A. E., Malaska, M. J., Continetti, R. E., et al. (2021b). Plume grain sampling at hypervelocity: Implications for astrobiology investigations. *Bull. AAS* 53. doi:10.3847/25c2cfeb.aef1b166

Čadek, O., Tobie, G., Van Hoolst, T., Massé, M., Choblet, G., Lefèvre, A., et al. (2016). Enceladus's internal ocean and ice shell constrained from Cassini gravity, shape, and libration data. *Geophys. Res. Lett.* 43, 5653–5660. doi:10.1002/2016GL068634

Cao, X., Bao, H., and Peng, Y. (2019). A kinetic model for isotopologue signatures of methane generated by biotic and abiotic CO2 methanation. *Geochimica Cosmochimica Acta* 249, 59–75. doi:10.1016/j.gca.2019.01.021

Choukroun, M., Backes, P., Cable, M. L., Hodyss, R., Badescu, M., Molaro, J. L., et al. (2021). Sampling ocean materials, traces of life or biosignatures in plume deposits on Enceladus' surface. *Bull. AAS* 53. doi:10.3847/25c2cfeb.78e80c4f

COSPAR, Committee on Space Research (2021). *COSPAR policy on planetary protection*. Availableat: https://cosparhq.cnes.fr/scientific-structure/panels/panel-onplanetary-protection-ppp/.

Cruikshank, D. P. (1980). Near-infrared studies of the satellites of Saturn and uranus. *Icarus* 41, 246–258. doi:10.1016/0019-1035(80)90008-1

Davis, D. C., Phillips, S. M., and McCarthy, B. P. (2018). Trajectory design for Saturnian Ocean Worlds orbiters using multidimensional Poincaré maps. *Acta Astronaut.* 143, 16–28. doi:10.1016/j.actaastro.2017.11.004

Dawson, P. B., Benítez, M. C., Lowenstern, J. B., and Chouet, B. A. (2012). Identifying bubble collapse in a hydrothermal system using hidden Markov models. *Geophys. Res. Lett.* 39. doi:10.1029/2011GL049901

Domagal-Goldman, S. D., Wright, K. E., Adamala, K., Arina de la Rubia, L., Bond, J., Dartnell, L. R., et al. (2016). The astrobiology primer v2.0. *Astrobiology* 16, 561–653. doi:10.1089/ast.2015.1460

Dombard, A. J., and Sessa, A. M. (2019). Gravity measurements are key in addressing the habitability of a subsurface ocean in Jupiter's Moon Europa. *Icarus* 325, 31–38. doi:10.1016/j.icarus.2019.02.025

Dooley, J. (2018). "Mission concept for a Europa lander," in 2018 IEEE Aerospace Conference, 1–10. doi:10.1109/AERO.2018.8396518

Dorn, E. D., Nealson, K. H., and Adami, C. (2011). Monomer abundance distribution patterns as a universal biosignature: Examples from terrestrial and digital life. *J. Mol. Evol.* 72, 283–295. doi:10.1007/s00239-011-9429-4

Duteïs, P., BrochardTiberio, R. S., Djafari-Rouhani, D., and Sanchez-Gestido, M. (2019). "Genevis: Generic vision-based navigation technology building blocks for space applications," in Proceedings of the GR740 User Day.

Ermakov, A. I., Park, R. S., Roa, J., Castillo-Rogez, J. C., Keane, J. T., Nimmo, F., et al. (2021). A recipe for the geophysical exploration of Enceladus. *Planet. Sci. J.* 2, 157. doi:10.3847/PSJ/ac06d2

Fabiani, G. P., and Costabile, V. (1997). Cassini HGA/LGAI antenna: When thermal design is a project driver. *Sixth Eur. Symposium Space Environ. Control Syst.* 400, 101. 1997ESASP.400.101F.

Fantino, E., Salazar, F., and Alessi, E. M. (2020). Design and performance of low-energy orbits for the exploration of Enceladus. *Commun. Nonlinear Sci. Numer. Simul.* 90, 105393. doi:10.1016/j.cnsns.2020.105393

Gautier, D., and Ip, W. H. (1984). Project Cassini: A Saturn orbiter/titan probe mission proposal. *Orig. Life* 14, 801–807. doi:10.1007/BF00933736

Georgiou, C. D., and Deamer, D. W. (2014). Lipids as universal biomarkers of extraterrestrial life. *Astrobiology* 14, 541–549. doi:10.1089/ast.2013.1134

Glavin, D. P., Burton, A. S., Elsila, J. E., Aponte, J. C., and Dworkin, J. P. (2020). The search for chiral asymmetry as a potential biosignature in our solar system. *Chem. Rev.* 120, 4660–4689. doi:10.1021/acs.chemrev.9b00474

Glein, C. R., Baross, J. A., and Waite, J. H. (2015). The pH of Enceladus' ocean. *Geochimica Cosmochimica Acta* 162, 202–219. doi:10.1016/j.gca.2015.04.017

Glein, C. R., Postberg, F., and Vance, S. D. (2018). "The geochemistry of Enceladus: Composition and controls," in *Enceladus and the icy moons of Saturn* (Tucson: Univ. of Arizona), 39–56.

Glein, C. R., and Waite, J. H. (2020). The carbonate geochemistry of Enceladus' ocean. *Geophys. Res. Lett.* 47, e2019GL085885. doi:10.1029/2019GL085885

Goesmann, F., Brinckerhoff, W. B., Raulin, F., Goetz, W., Danell, R. M., Getty, S. A., et al. (2017). The Mars Organic Molecule Analyzer (MOMA) instrument: Characterization of organic material in martian sediments. *Astrobiology* 17, 655–685. doi:10.1089/ast.2016.1551

Goguen, J. D., Buratti, B. J., Brown, R. H., Clark, R. N., Nicholson, P. D., Hedman, M. M., et al. (2013). The temperature and width of an active fissure on Enceladus measured with Cassini VIMS during the 14 April 2012 South Pole flyover. *Icarus* 226, 1128–1137. doi:10.1016/j.icarus.2013.07.012

Gómez-Elvira, J., Armiens, C., Castañer, L., Domínguez, M., Genzer, M., Gómez, F., et al. (2012). Rems: The environmental sensor suite for the Mars science laboratory rover. *Space Sci. Rev.* 170, 583–640. doi:10.1007/s11214-012-9921-1

Guzman, M., Lorenz, R., Hurley, D., Farrell, W., Spencer, J., Hansen, C., et al. (2019). Collecting amino acids in the Enceladus plume. *Int. J. Astrobiol.* 18, 47–59. doi:10.1017/S1473550417000544

Hajdik, H., Ramsey, S., Wright, R. A., Stover, N., Patel, J., Spitznas, J., et al. (2020). *Titan aerogravity assist for Saturn orbital insertion and study of Enceladus. Chancellor's honors program projects*. Availableat: https://trace.tennessee.edu/utk_chanhonoproj/2396.

Hand, K. P., Murray, A. E., and Garvin, J. B. (2017). *Report of the Europa lander science definition team*. Availableat: https://europa.nasa.gov/resources/58/europa-lander-study-2016-report/.Europa lander SDT

Hand, K. P., Phillips, C. B., Murray, A., Garvin, J. B., Maize, E. H., Gibbs, R. G., et al. (2022). Science goals and mission architecture of the Europa lander mission concept. *Planet. Sci. J.* 3, 22. doi:10.3847/PSJ/ac4493

Hansen, C. J., Esposito, L., Stewart, A. I. F., Colwell, J., Hendrix, A., Pryor, W., et al. (2006). Enceladus' water vapor plume. *Science* 311, 1422–1425. doi:10.1126/science.1121254

Hansen, C. J., Esposito, L. W., Colwell, J. E., Hendrix, A. R., Portyankina, G., Stewart, A. I. F., et al. (2020). The composition and structure of Enceladus' plume from the complete set of Cassini UVIS occultation observations. *Icarus* 344, 113461. doi:10.1016/j.icarus.2019.113461

Hansen, C. J., Shemansky, D. E., Esposito, L. W., Stewart, A. I. F., Lewis, B. R., Colwell, J. E., et al. (2011). The composition and structure of the Enceladus plume. *Geophys. Res. Lett.* 38. doi:10.1029/2011GL047415

Hedman, M. M., Gosmeyer, C. M., Nicholson, P. D., Sotin, C., Brown, R. H., Clark, R. N., et al. (2013). An observed correlation between plume activity and tidal stresses on Enceladus. *Nature* 500, 182–184. doi:10.1038/nature12371

Heffels, A., Knapmeyer, M., Oberst, J., and Haase, I. (2017). Re-Evaluation of Apollo 17 lunar seismic profiling experiment data. *Planet. Space Sci.* 135, 43–54. doi:10.1016/j.pss.2016.11.007

Heffels, A., Knapmeyer, M., Oberst, J., and Haase, I. (2021). Re-Evaluation of Apollo 17 lunar seismic profiling experiment data including new LROC-derived coordinates for explosive packages 1 and 7, at taurus-littrow, moon. *Planet. Space Sci.* 206, 105307. doi:10.1016/j.pss.2021.105307

Hemingway, D. J., and Mittal, T. (2019). Enceladus's ice shell structure as a window on internal heat production. *Icarus* 332, 111–131. doi:10.1016/j.icarus.2019.03.011

Henin, B. (2018). "Enceladus," in *Exploring the ocean worlds of our solar system Astronomers' universe*. Editor B. Henin (Cham: Springer International Publishing), 159–188. doi:10.1007/978-3-319-93476-1_8

Henry, C. A. (2003). "An introduction to the design of the Cassini spacecraft," in *The cassini-huygens mission: Overview, objectives and huygens instrumentarium volume 1*. Editor C. T. Russell (Dordrecht: Springer Netherlands), 129–153. doi:10.1007/978-94-017-3251-2_4

Higgs, P. G., and Pudritz, R. E. (2009). A thermodynamic basis for prebiotic amino acid synthesis and the nature of the first genetic code. *Astrobiology* 9, 483–490. doi:10.1089/ast.2008.0280

Hill, J. (2000). *Sulfur and the origins of life*. Masters Thesis. Christchurch: University of Canterbury. doi:10.26021/7093

Hoehler, T., Brinckerhoff, W., Davila, A., Marais, D. D., Getty, S., Glavin, D., et al. (2021). Groundwork for life detection. *Bull. AAS* 53. doi:10.3847/25c2cfeb.bd9172f9

Hou, Y., Jiao, R., and Yu, H. (2021). MEMS based geophones and seismometers. *Sensors Actuators A Phys.* 318, 112498. doi:10.1016/j.sna.2020.112498

Hsu, H.-W., Postberg, F., Sekine, Y., Shibuya, T., Kempf, S., Horányi, M., et al. (2015). Ongoing hydrothermal activities within Enceladus. *Nature* 519, 207–210. doi:10.1038/nature14262

Hurford, T. A., Helfenstein, P., Hoppa, G. V., Greenberg, R., and Bills, B. G. (2007). Eruptions arising from tidally controlled periodic openings of rifts on Enceladus. *Nature* 447, 292–294. doi:10.1038/nature05821

Iess, L., Stevenson, D. J., Parisi, M., Hemingway, D., Jacobson, R. A., Lunine, J. I., et al. (2014). The gravity field and interior structure of Enceladus. *Science* 344, 78–80. doi:10.1126/science.1250551

James, N., Abello, R., Lanucara, M., Mercolino, M., and Maddè, R. (2009). Implementation of an ESA delta-DOR capability. *Acta Astronaut.* 64, 1041–1049. doi:10.1016/j.actaastro.2009.01.005

Jaramillo-Botero, A., Cable, M. L., Hofmann, A. E., Malaska, M., Hodyss, R., and Lunine, J. (2021). Understanding hypervelocity sampling of biosignatures in space missions. *Astrobiology* 21, 421–442. doi:10.1089/ast.2020.2301

Jaumann, R., Stephan, K., Hansen, G. B., Clark, R. N., Buratti, B. J., Brown, R. H., et al. (2008). Distribution of icy particles across Enceladus' surface as derived from Cassini-VIMS measurements. *Icarus* 193, 407–419. doi:10.1016/j.icarus.2007.09.013

Jones, D. H., and Gudmundsson, G. H. (2013). Aircraft-deployable ice observation system (ADIOS) for instrumenting inaccessible glaciers. *J. Glaciol.* 59, 1129–1134. doi:10.3189/2013JoG13J112

Jones, S. M., and Sakamotot, J. (2006). Aerogel: Space exploration applications. *J. Solgel. Sci. Technol.* 40 (2), 351–357. doi:10.1007/s10971-006-7762-7

Kahana, A., Schmitt-Kopplin, P., and Lancet, D. (2019). Enceladus: First observed primordial soup could arbitrate origin-of-life debate. *Astrobiology* 19, 1263–1278. doi:10.1089/ast.2019.2029

Kanani, K., Brochard, R., Hennart, F., Pollini, A., Sturm, P., Dubois-Matra, O., et al. (2016). *Sensor data fusion for hazard mapping and piloting*. Availableat: https://hal.inria.fr/hal-01396797.

Kang, W., Mittal, T., Bire, S., Campin, J.-M., and Marshall, J. (2022). How does salinity shape ocean circulation and ice geometry on Enceladus and other icy satellites? *Sci. Adv.* 8, eabm4665. doi:10.1126/sciadv.abm4665

Karatekin, Ö., Mimoun, D., Murdoch, N., Eubanks, M., Carrasco, J., Vasseur, H., et al. (2016). *The Asteroid Geophysical Explorer (AGEX); A proposal to explore Didymos system using cubesats*. EGU General Assembly Vol. 18 abstract 17097.

Kargel, J. S., and Pozio, S. (1996). The volcanic and tectonic history of Enceladus. *Icarus* 119, 385–404. doi:10.1006/icar.1996.0026

Kirchoff, M. R., and Schenk, P. (2009). Crater modification and geologic activity in Enceladus' heavily cratered plains: Evidence from the impact crater distribution. *Icarus* 202, 656–668. doi:10.1016/j.icarus.2009.03.034

Klenner, F., Postberg, F., Hillier, J., Khawaja, N., Cable, M. L., Abel, B., et al. (2020). Discriminating abiotic and biotic fingerprints of amino acids and fatty acids in ice grains relevant to ocean worlds. *Astrobiology* 20, 1168–1184. doi:10.1089/ast.2019.2188

Kliore, A. J., Anderson, J. D., Armstrong, J. W., Asmar, S. W., Hamilton, C. L., Rappaport, N. J., et al. (2004). "Cassini radio science," in *The cassini-huygens mission: Orbiter remote sensing investigations*. Editor C. T. Russell (Dordrecht: Springer Netherlands), 1–70. doi:10.1007/1-4020-3874-7_1

Knoll, A. H. (2003). The geological consequences of evolution. *Geobiology* 1, 3–14. doi:10.1046/j.1472-4669.2003.00002.x

Koh, Z.-W., Nimmo, F., Lunine, J. I., Mazarico, E., and Dombard, A. J. (2022). Assessing the detectability of Europa's seafloor topography from Europa Clipper's gravity data. *Planet. Sci. J.* 3, 197. doi:10.3847/PSJ/ac82aa

Konstantinidis, K., Flores Martinez, C. L., Dachwald, B., Ohndorf, A., Dykta, P., Bowitz, P., et al. (2015). A lander mission to probe subglacial water on Saturn's moon Enceladus for life. *Acta Astronaut.* 106, 63–89. doi:10.1016/j.actaastro.2014.09.012

Le Gall, A., Leyrat, C., Janssen, M. A., Choblet, G., Tobie, G., Bourgeois, O., et al. (2017). Thermally anomalous features in the subsurface of Enceladus's south polar terrain. *Nat. Astron.* 1, 0063–0065. doi:10.1038/s41550-017-0063

Lebreton, J., Brochard, R., Baudry, M., Jonniaux, G., Salah, A. H., Kanani, K., et al. (2021). *Image simulation for space applications with the SurRender software*. doi:10.48550/arXiv.2106.11322

Lee, A. Y., and Burk, T. A. (2019). Cassini spacecraft attitude control system performance and lessons learned, 1997–2017. *J. Spacecr. Rockets* 56, 158–170. doi:10.2514/1.A34236

Leeds, M. W., Eberhardt, R. N., and Berry, R. L. (1996). Development of the Cassini spacecraft propulsion subsystem. Available at: https://trs.jpl.nasa.gov/handle/2014/26073.

MacKenzie, S. M., Neveu, M., Davila, A. F., Lunine, J. I., Craft, K. L., Cable, M. L., et al. (2021). The Enceladus Orbilander mission concept: Balancing return and resources in the search for life. *Planet. Sci. J.* 2, 77. doi:10.3847/PSJ/abe4da

MacKenzie, S. M., Neveu, M., Lunine, J. I., and Davila, A. F. (2020). Enceladus orbilander: A flagship mission concept for astrobiology. *Planet. Mission. Concept Study*. Available at: https://lib.jhuapl.edu/papers/the-enceladus-orbilander/.

Marshall, S. M., Murray, A. R. G., and Cronin, L. (2017). A probabilistic framework for identifying biosignatures using Pathway Complexity. *Phil. Trans. R. Soc. A* 375, 20160342. doi:10.1098/rsta.2016.0342

Martens, H. R., Ingersoll, A. P., Ewald, S. P., Helfenstein, P., and Giese, B. (2015). Spatial distribution of ice blocks on Enceladus and implications for their origin and emplacement. *Icarus* 245, 162–176. doi:10.1016/j.icarus.2014.09.035

Martin, W., Baross, J., Kelley, D., and Russell, M. J. (2008). Hydrothermal vents and the origin of life. *Nat. Rev. Microbiol.* 6, 805–814. doi:10.1038/nrmicro1991

Martin, W., and Russell, M. J. (2007). On the origin of biochemistry at an alkaline hydrothermal vent. *Phil. Trans. R. Soc. B* 362, 1887–1926. doi:10.1098/rstb.2006.1881

Massarweh, L., and Cappuccio, P. (2020). "On the restricted 3-body problem for the saturn-enceladus system: Mission geometry & orbit design for plume sampling missions," in *AIAA scitech 2020 forum AIAA SciTech forum* (American Institute of Aeronautics and Astronautics). doi:10.2514/6.2020-0467

Mathies, R., and Butterworth, A. (2021). The case for an orbital mission to characterize the organic content of the Enceladus plumes. *Bull. AAS* 53. doi:10.3847/25c2cfeb.94bb9acc

Matson, D. L., Castillo, J. C., Lunine, J., and Johnson, T. V. (2007). Enceladus' plume: Compositional evidence for a hot interior. *Icarus* 187, 569–573. doi:10.1016/j.icarus.2006.10.016

Matson, D. L., Castillo-Rogez, J. C., Davies, A. G., and Johnson, T. V. (2012). Enceladus: A hypothesis for bringing both heat and chemicals to the surface. *Icarus* 221, 53–62. doi:10.1016/j.icarus.2012.05.031

McKay, C. P., Anbar, A. D., Porco, C., and Tsou, P. (2014). Follow the plume: The habitability of Enceladus. *Astrobiology* 14, 352–355. doi:10.1089/ast.2014.1158

McKay, C. P., Porco, C. C., Altheide, T., Davis, W. L., and Kral, T. A. (2008). The possible origin and persistence of life on Enceladus and detection of biomarkers in the plume. *Astrobiology* 8, 909–919. doi:10.1089/ast.2008.0265

McKay, D. S., Gibson, E. K., Thomas-Keprta, K. L., Vali, H., Romanek, C. S., Clemett, S. J., et al. (1996). Search for past life on Mars: Possible relic biogenic activity in martian meteorite ALH84001. *Science* 273, 924–930. doi:10.1126/science.273.5277.924

McKinnon, W. B. (2015). Effect of Enceladus's rapid synchronous spin on interpretation of Cassini gravity. *Geophys. Res. Lett.* 42, 2137–2143. doi:10.1002/2015GL063384

Mizutani, H., Kohno, M., Nakajima, S., Fujimura, A., Kawaguchi, J., Saito, H., et al. (1995). Japanese lunar mission, LUNAR-A. *Acta Astronaut.* 35, 323–327. doi:10.1016/0094-5765(94)00197-T

Mizutani, H. (1995). Lunar interior exploration by Japanese lunar penetrator mission, LUNAR-A. *JPhysEarth.* 43 (5), 657–670. doi:10.4294/jpe1952.43.657

Mottola, S., Arnold, G., Grothues, H.-G., Jaumann, R., Michaelis, H., Neukum, G., et al. (2007). The rolis experiment on the Rosetta lander. *Space Sci. Rev.* 128, 241–255. doi:10.1007/s11214-006-9004-2

Nathan, E., Balachandran, K., Cappuccio, P., Di, J., Doerkson, K., Gloder, A., et al. (2022). A multi-lander new Frontiers mission concept study for Enceladus: Silenus. *Front. Astron. Space Sci.* 9. doi:10.3389/fspas.2022.995941

Neveu, M., Hays, L. E., Voytek, M. A., New, M. H., and Schulte, M. D. (2018). The ladder of life detection. *Astrobiology* 18, 1375–1402. doi:10.1089/ast.2017.1773

Neveu, S. (2016). Informing Mars sample selection strategies: Identifying fossil biosignatures and assessing their preservation potential. Ph.D. Thesis. Available at: https://ui.adsabs.harvard.edu/abs/2016PhDT.....114N.

New, J. S., Kazemi, B., Spathis, V., Price, M. C., Mathies, R. A., and Butterworth, A. L. (2021). Quantitative evaluation of the feasibility of sampling the ice plumes at Enceladus for biomarkers of extraterrestrial life. *Proc. Natl. Acad. Sci. U. S. A.* 118, e2106197118. doi:10.1073/pnas.2106197118

Nimmo, F., Bills, B. G., and Thomas, P. C. (2011). Geophysical implications of the long-wavelength topography of the Saturnian satellites. *J. Geophys. Res.* 116, E11001. doi:10.1029/2011JE003835

Nimmo, F., Porco, C., and Mitchell, C. (2014). Tidally modulated eruptions on Enceladus: Cassini ISS observations and models. *Astron. J.* 148, 46. doi:10.1088/0004-6256/148/3/46

Northey, J., and Kinney, S. (2014). *Guidelines for risk management. Independent verification and validation program*, 19. Version: F, 2014. Available at: https://www.nasa.gov/sites/default/files/atoms/files/ivv_s3001_-_ver_f.pdf.

NRC (2022). *Origins, worlds, and life: A decadal strategy for planetary science and astrobiology 2023-2032*. National Academies. doi:10.17226/26522

NRC (2011). *Vision and Voyages for planetary science in the decade 2013-2022*. National Academies. doi:10.17226/13117

Nunn, C., Garcia, R. F., Nakamura, Y., Marusiak, A. G., Kawamura, T., Sun, D., et al. (2020). Lunar seismology: A data and instrumentation review. *Space Sci. Rev.* 216, 89. doi:10.1007/s11214-020-00709-3

Pajola, M., Lucchetti, A., Semenzato, A., Poggiali, G., Munaretto, G., Galluzzi, V., et al. (2021). Lermontov crater on Mercury: Geology, morphology and spectral properties of the coexisting hollows and pyroclastic deposits. *Planet. Space Sci.* 195, 105136. doi:10.1016/j.pss.2020.105136

Panning, M., and Romanowicz, B. (2006). A three-dimensional radially anisotropic model of shear velocity in the whole mantle. *Geophys. J. Int.* 167, 361–379. doi:10.1111/j.1365-246X.2006.03100.x

Park, R. S., Riedel, J. E., Ermakov, A. I., Roa, J., Castillo-Rogez, J., Davies, A. G., et al. (2020). Advanced Pointing Imaging Camera (APIC) for planetary science and mission opportunities. *Planet. Space Sci.* 194, 105095. doi:10.1016/j.pss.2020.105095

Parkinson, C. D., Liang, M.-C., Yung, Y. L., and Kirschivnk, J. L. (2008). Habitability of Enceladus: Planetary conditions for life. *Orig. Life Evol. Biosph.* 38, 355–369. doi:10.1007/s11084-008-9135-4

Pope, E. C., Bird, D. K., and Rosing, M. T. (2012). Isotope composition and volume of Earth's early oceans. *Proc. Natl. Acad. Sci. U. S. A.* 109, 4371–4376. doi:10.1073/pnas.1115705109

Porco, C. C., Dones, L., and Mitchell, C. (2017). Could it Be snowing microbes on Enceladus? Assessing conditions in its plume and implications for future missions | astrobiology. *Astrobiology* 17, 876–901. doi:10.1089/ast.2017.1665

Porco, C. C., Helfenstein, P., Thomas, P. C., Ingersoll, A. P., Wisdom, J., West, R., et al. (2006). Cassini observes the active south Pole of Enceladus. *Science* 311, 1393–1401. doi:10.1126/science.1123013

Porco, C., DiNino, D., and Nimmo, F. (2014). How the geysers, tidal stresses, and thermal emission across the south polar terrain of Enceladus are related. *Astron. J.* 148, 45. doi:10.1088/0004-6256/148/3/45

Postberg, F., Khawaja, N., Abel, B., Choblet, G., Glein, C. R., Gudipati, M. S., et al. (2018). Macromolecular organic compounds from the depths of Enceladus. *Nature* 558, 564–568. doi:10.1038/s41586-018-0246-4

Postberg, F., Schmidt, J., Hillier, J., Kempf, S., and Srama, R. (2011). A salt-water reservoir as the source of a compositionally stratified plume on Enceladus. *Nature* 474, 620–622. doi:10.1038/nature10175

Rabinovitch, J., Mihaly, J., Parziale, N., Mehrotra, P., Cymbalist, N., Burgoyne, H., et al. (2014). "The Caltech space challenge: Lessons learned and future plans," in 65th International Astronautical Congress.

Reuter, D. C., Stern, S. A., Scherrer, J., Jennings, D. E., Baer, J. W., Hanley, J., et al. (2008). Ralph: A visible/infrared imager for the new horizons pluto/kuiper belt mission. *Space Sci. Rev.* 140, 129–154. doi:10.1007/s11214-008-9375-7

Roberts, J. H., and Nimmo, F. (2008). Near-surface heating on Enceladus and the south polar thermal anomaly. *Geophys. Res. Lett.* 35, L09201. doi:10.1029/2008GL033725

Russell, M. J., Barge, L. M., Bhartia, R., Bocanegra, D., Bracher, P. J., Branscomb, E., et al. (2014). The drive to life on wet and icy worlds. *Astrobiology* 14, 308–343. doi:10.1089/ast.2013.1110

Russell, R. P., and Lara, M. (2009). On the design of an Enceladus science orbit. *Acta Astronaut.* 65, 27–39. doi:10.1016/j.actaastro.2009.01.021

Schmidt, J., Brilliantov, N., Spahn, F., and Kempf, S. (2008). Slow dust in Enceladus' plume from condensation and wall collisions in tiger stripe fractures. *Nature* 451, 685–688. doi:10.1038/nature06491

Schmidt, T. M., and Bhandari, P. (2019). "Thermal design of a Europa lander mission concept," in 49th International Conference on Environmental Systems (Pasadena: ICES-2019-4).

Schopf, J. W. (1993). Microfossils of the early archean apex chert: New evidence of the antiquity of life. *Science* 260, 640–646. doi:10.1126/science.260.5108.640

Sebastián, E., Armiens, C., Gómez-Elvira, J., Zorzano, M. P., Martinez-Frias, J., Esteban, B., et al. (2010). The rover environmental monitoring station ground temperature sensor: A pyrometer for measuring ground temperature on Mars. *Sensors* 10, 9211–9231. doi:10.3390/s101009211

Shields, A., Garcia, A., Nawotniak, S. K., Lim, D. S. S., and Raineault, N. (2019). *Discovering the Apollo deep sea hydrothermal vent field at Northern Gorda Ridge, using bathymetric data*. American Geophysical Union, Fall Meeting 2019, abstract #OS13C-1557.

Shuai, Y., Etiope, G., Zhang, S., Douglas, P. M. J., Huang, L., and Eiler, J. M. (2018). Methane clumped isotopes in the Songliao Basin (China): New insights into abiotic vs. biotic hydrocarbon formation. *Earth Planet. Sci. Lett.* 482, 213–221. doi:10.1016/j.epsl.2017.10.057

Simoneit, B. R. T. (2004). Biomarkers (molecular fossils) as geochemical indicators of life. *Adv. Space Res.* 33, 1255–1261. doi:10.1016/j.asr.2003.04.045

Simoneit, B. R. T. (2002). Molecular indicators (biomarkers) of past life. *Anat. Rec. Hob.* 268, 186–195. doi:10.1002/ar.10153

Smith, B. A., Soderblom, L., Batson, R., Bridges, P., Inge, J., Masursky, H., et al. (1982). A new look at the Saturn system: The Voyager 2 images. *Science* 215, 504–537. doi:10.1126/science.215.4532.504

Sollberger, D., Schmelzbach, C., Robertsson, J. O. A., Greenhalgh, S. A., Nakamura, Y., and Khan, A. (2016). The shallow elastic structure of the lunar crust: New insights from seismic wavefield gradient analysis. *Geophys. Res. Lett.* 43 (10), 10,078–10,087. doi:10.1002/2016GL070883

Sornsin, B. A., Short, B. W., Bourbeau, T. N., and Dahlin, M. J. (2019). Global shutter solid state flash lidar for spacecraft navigation and docking applications. *Laser Radar Technol. Appl.* XXIV, 229–240. doi:10.1117/12.2519178

Southworth, B. S., Kempf, S., and Spitale, J. (2019). Surface deposition of the Enceladus plume and the zenith angle of emissions. *Icarus* 319, 33–42. doi:10.1016/j.icarus.2018.08.024

Spahn, F., Schmidt, J., Albers, N., Hörning, M., Makuch, M., Seiß, M., et al. (2006). Cassini dust measurements at Enceladus and implications for the origin of the E ring. *Science* 311, 1416–1418. doi:10.1126/science.1121375

Spencer, J. R., and Nimmo, F. (2013). Enceladus: An active ice world in the Saturn system. *Annu. Rev. Earth Planet. Sci.* 41, 693–717. doi:10.1146/annurev-earth-050212-124025

Stephens, S. K. (2015). "The Juno mission to Jupiter: Lessons from cruise and plans for orbital operations and science return," in 2015 IEEE Aerospace Conference, 1–20. doi:10.1109/AERO.2015.7118972

Stern, S. A., Slater, D. C., Scherrer, J., Stone, J., Dirks, G., Versteeg, M., et al. (2009). "Alice: The ultraviolet imaging spectrograph aboard the new horizons pluto–kuiper belt mission," in *New horizons: Reconnaissance of the pluto-charon system and the kuiper belt*. Editor C. T. Russell (New York, NY: Springer), 155–187. doi:10.1007/978-0-387-89518-5_8

Stoeckenius, W. (1962). "The molecular structure of lipid-water sytems and cell membrane models studied with the electron microscope," in *The interpretation of ultrastructure international society for cell biology symposia*. Editor R. J. C. Harris (Academic Press), 349–367. doi:10.1016/B978-1-4832-3079-5.50022-9

Summons, R. E., Albrecht, P., McDonald, G., and Moldowan, J. M. (2008). "Molecular biosignatures," in *Strategies of life detection space sciences series of ISSI*. Editors O. Botta, J. L. Bada, J. Gomez-Elvira, E. Javaux, F. Selsis, and R. Summons (Boston, MA: Springer US), 133–159. doi:10.1007/978-0-387-77516-6_11

Surampudi, R., Bugga, K., Brandon, E., Elliott, J., and Beauchamp, P. (2018). *Advanced energy storage technologies for future NASA planetary science missions*, 53.

Sverjensky, D. A., and Lee, N. (2010). The great oxidation event and mineral diversification. *Elements* 6, 31–36. doi:10.2113/gselements.6.1.31

Tajeddine, R., Soderlund, K. M., Thomas, P. C., Helfenstein, P., Hedman, M. M., Burns, J. A., et al. (2017). True polar wander of Enceladus from topographic data. *Icarus* 295, 46–60. doi:10.1016/j.icarus.2017.04.019

Taylor, J., Sakamoto, L., and Wong, C. J. (2002). *Cassini orbiter/huygens probe telecommunications, descanso design and performance summary series*. Pasadena, California.

Teolis, B. D., Perry, M. E., Magee, B. A., Westlake, J., and Waite, J. H. (2010). Detection and measurement of ice grains and gas distribution in the Enceladus plume by Cassini's Ion Neutral Mass Spectrometer. *J. Geophys. Res.* 115. doi:10.1029/2009JA015192

Thomas, P. C., Tajeddine, R., Tiscareno, M. S., Burns, J. A., Joseph, J., Loredo, T. J., et al. (2016). Enceladus's measured physical libration requires a global subsurface ocean. *Icarus* 264, 37–47. doi:10.1016/j.icarus.2015.08.037

Thornton, C. L., and Border, J. S. (2003). *Radiometric tracking techniques for deep-space navigation* | Wiley. Available at: https://www.wiley.com/en-us/Radiometric+Tracking+Techniques+for+Deep+Space+Navigation-p-9780471445340.

Tian, F., Stewart, A. I. F., Toon, O. B., Larsen, K. W., and Esposito, L. W. (2007). Monte Carlo simulations of the water vapor plumes on Enceladus. *Icarus* 188, 154–161. doi:10.1016/j.icarus.2006.11.010

Tokar, R. L., Johnson, R. E., Thomsen, M. F., Wilson, R. J., Young, D. T., Crary, F. J., et al. (2009). Cassini detection of Enceladus' cold water-group plume ionosphere. *Geophys. Res. Lett.* 36, L13203. doi:10.1029/2009GL038923

Tyler, R. H. (2009). Ocean tides heat Enceladus. *Geophys. Res. Lett.* 36. doi:10.1029/2009GL038300

Vance, S., Běhounková, M., Bills, B. G., Byrne, P., Čadek, O., Castillo-Rogez, J., et al. (2021). Distributed geophysical exploration of Enceladus and other ocean worlds. *Bull. AAS* 53. doi:10.3847/25c2cfeb.a07234f4

Vance, S. D., Hand, K. P., and Pappalardo, R. T. (2016). Geophysical controls of chemical disequilibria in Europa. *Geophys. Res. Lett.* 43, 4871–4879. doi:10.1002/2016GL068547

Vance, S. D., Panning, M. P., Stähler, S., Cammarano, F., Bills, B. G., Tobie, G., et al. (2018). Geophysical investigations of habitability in ice-covered ocean worlds. *JGR. Planets* 123, 180–205. doi:10.1002/2017JE005341

Verbiscer, A. J., French, R. G., and McGhee, C. A. (2005). The opposition surge of Enceladus: HST observations 338–1022 nm. *Icarus* 173, 66–83. doi:10.1016/j.icarus.2004.05.001

Waite, J. H., Combi, M. R., Ip, W.-H., Cravens, T. E., McNutt, R. L., Kasprzak, W., et al. (2006). Cassini ion and neutral mass spectrometer: Enceladus plume composition and structure. *Science* 311, 1419–1422. doi:10.1126/science.1121290

Waite, J. H., Glein, C. R., Perryman, R. S., Teolis, B. D., Magee, B. A., Miller, G., et al. (2017). Cassini finds molecular hydrogen in the Enceladus plume: Evidence for hydrothermal processes. *Science* 356, 155–159. doi:10.1126/science.aai8703

Waite, J. H., Lewis, W. S., Magee, B. A., Lunine, J. I., McKinnon, W. B., Glein, C. R., et al. (2009). Liquid water on Enceladus from observations of ammonia and 40Ar in the plume. *Nature* 460, 487–490. doi:10.1038/nature08153

Watteau, F., and Villemin, G. (2018). Soil microstructures examined through transmission electron microscopy reveal soil-microorganisms interactions. *Front. Environ. Sci.* 6. 10.3389/fenvs.2018.00106.

Weiss, J. M., and Guernsey, C. S. (2013). Design and development of the MSL descent stage propulsion system. Available at: https://trs.jpl.nasa.gov/handle/2014/44893.

Woerner, D., Moreno, V., Jones, L., Zimmerman, R., and Wood, E. (2013). The Mars science laboratory (msl) MMRTG in-flight: A power update. Availableat: http://hdl.handle.net/2014/44945.

Woerner, D. (2017). "Next generation RTGs for NASA," in 15th International Energy Conversion Engineering Conference, 4612. Availableat: http://hdl.handle.net/2014/46421.

Wu, S.-M., Lin, F.-C., Farrell, J., Shiro, B., Karlstrom, L., Okubo, P., et al. (2020). Spatiotemporal seismic structure variations associated with the 2018 kīlauea eruption based on temporary dense geophone arrays. *Geophys. Res. Lett.* 47, e2019GL086668. doi:10.1029/2019GL086668

Yeoh, S. K., Chapman, T. A., Goldstein, D. B., Varghese, P. L., and Trafton, L. M. (2015). On understanding the physics of the Enceladus south polar plume via numerical simulation. *Icarus* 253, 205–222. doi:10.1016/j.icarus.2015.02.020

Zandanel, A., Truche, L., Hellmann, R., Myagkiy, A., Choblet, G., and Tobie, G. (2021). Short lifespans of serpentinization in the rocky core of Enceladus: Implications for hydrogen production. *Icarus* 364, 114461. doi:10.1016/j.icarus.2021.114461

Zolotov, M. Y. (2007). An oceanic composition on early and today's Enceladus. *Geophys. Res. Lett.* 34. doi:10.1029/2007GL031234